Journal of Environmental Management 376 (2025) 124446



Contents lists available at ScienceDirect

Journal of Environmental Management

journal homepage: www.elsevier.com/locate/jenvman



Research article

Green infrastructure and its influence on urban heat island, heat risk, and air pollution: A case study of Porto (Portugal)

Hélder Silva Lopes [a,b,c,*], Diogo Guedes Vidal [c,d], Nadhima Cherif [e,f], Lígia Silva [a,f], Paula C. Remoaldo [a]

[a] Lab2PT – Landscape, Heritage and Territory Laboratory/IN2PAST/Department of Geography /ICS, University of Minho, Guimarães, Portugal
[b] IdRA – Climatology Group/ Department of Geography/FGH, University of Barcelona, Barcelona, Spain
[c] Higher School of Education Paula Frassinetti (ESEPF), Porto, Portugal
[d] Centre for Functional Ecology—Science for People and the Planet (CFE), Associate Laboratory TERRA, Department of Life Sciences (DCV), University of Coimbra, Coimbra, Portugal
[e] Laboratory for Management and Control of Animal and Environmental Resources in Semi-Arid Environments, Higher Agronomic Institute of Chott Meriem, Sousse, Tunisia
[f] Centre for Territory, Environment and Construction (CTAC), School of Engineering, University of Minho, Guimarães, Portugal

ARTICLE INFO

Handling Editor: Dr. Lixiao Zhang

Keywords:
Urban heat island
Green infrastructure deprivation
Heat risk index
Air pollution
Urban resilience
Environmental justice

ABSTRACT

Green infrastructure plays a fundamental role in mitigating the effects of urban heat island. Vegetation may trap particulates and absorb pollutants like ozone, thus improving air quality. Understanding how green infrastructure reduces urban heat island and air pollution within specific urban zones can provide valuable insights for better urban design, improved environmental quality, and increased resident well-being. This study addresses the impact of green infrastructure deprivation on urban heat island effects, air pollution, and heat-related health risks in Porto, Portugal. The study employs a monitoring network to analyse the spatial distribution of air temperature and humidity throughout the city, although with specific gaps in coverage. With a focus on the role of urban green infrastructure in mitigating air urban heat island effects, this paper uses the data from Porto Digital's monitoring network between 2019 and 2022. Heat risk index assesses vulnerability to heat-related health risks by integrating land surface temperature, land cover, and demographic data through remote sensing. Green infrastructure mapping is conducted to quantify the spatial distribution of vegetation elements in the study area. The data analysis from 2019 to 2022 reveals that urban heat island intensity is more pronounced during the summer and at night. Approximately 32.6% of Porto is in areas with a high heat risk index, indicating increased vulnerability to heat-related health risks. The study finds that limited green infrastructure exacerbates this vulnerability, particularly in socioeconomically disadvantaged areas. Additionally, persistent air pollution hotspots, including elevated levels of ozone and particulate matter, contribute to the intensity of urban heat island. These findings underscore the need for integrating green infrastructure into urban planning to mitigate urban heat island and air pollution, improve urban resilience, and promote environmental justice.

1. Introduction

Global urbanisation has significantly altered population distribution, with projections indicating that by 2050, 68% of the world's population will reside in cities (Giles-Corti et al., 2020), a shift driven by improved employment opportunities and economic conditions (Falah et al., 2020; Naboni et al., 2019; Narimani et al., 2022; Oliveira et al., 2020; Vidal et al., 2019). This urbanisation brings significant challenges for urban climates, particularly the Urban Heat Island (UHI) effect. UHI refers to the higher temperatures in urban areas than their rural counterparts, driven by dense construction, energy consumption, and limited vegetation. The UHI effect intensifies the energy demand, worsens air quality, and increases the risk of heat-related health problems (Cetin, 2019; Chen et al., 2016; Dang et al., 2023; Kim and Brown, 2021; Tam et al.,

* Corresponding author. Lab2PT – Landscape, Heritage and Territory Laboratory/IN2PAST/Department of Geography /ICS, University of Minho, Guimarães, Portugal.
E-mail addresses: helderlopes@geografia.uminho.pt (H.S. Lopes), diogo.vidal@uc.pt (D.G. Vidal), cherif.nadhima2019@gmail.com (N. Cherif), lsilva@civil.uminho.pt (L. Silva), premoaldo@geografia.uminho.pt (P.C. Remoaldo).

https://doi.org/10.1016/j.jenvman.2025.124446
Received 14 May 2024; Received in revised form 9 January 2025; Accepted 1 February 2025
Available online 8 February 2025
0301-4797/© 2025 The Authors. Published by Elsevier Ltd. This is an open access article under the CC BY license (http://creativecommons.org/licenses/by/4.0/).

2015; Thuy et al., 2023). In addition, problems related to climate risks in urban areas led some authors to introduce the paradigm of resilience in risk adaptation (e.g. Martín and Paneque, 2022; Lopes et al., 2023). This paradigm asserted itself during the Sendai Conference in 2015 and implied a change from a negative to a positive view on people's adaptive and self-protective capacity (Lo et al., 2017; Wisner, 2016).

UHI conveys the notion of elevated temperatures within urban areas compared to their rural surroundings, with its impact often felt most strongly during nighttime (Lowry, 1977; Oke et al., 2017). However, this distinction is not solely a result of the urban lifestyle but rather arises from complex factors. A weather variable, as explained by the framework established by Lowry (1977) and later adopted by Oke et al. (2017), emerges as the sum of three components: (i) the fundamental macroclimate backdrop of the region, (ii) contributions stemming from geographical and landscape attributes, and (iii) effects arising from human activities and land use, including urban land cover. UHI pertains explicitly to the human component, signifying the contribution attributable to human activities and habitation, cautioning against the use of UHI terminology in scenarios influenced by intricate geographical and landscape controls, such as topography or proximity to the coastline (Lopes et al., 2021; Oke et al., 2017). Mitigating these effects is thus crucial for increasing urban livability and environmental quality.

Furthermore, combining UHI with air pollution is a significant concern in metropolitan areas. Higher temperatures caused by UHI can increase air pollution by increasing ground-level ozone and other pollutants (Arunab and Mathew, 2024). This interaction impacts environmental quality and poses serious public health hazards, particularly to vulnerable people (Cichowicz and Bochenek, 2024).

The human and non-human influences on local microclimate conditions have spurred studies aiming to guide designing higher-quality urban spaces. Of particular interest are the availability of Green Infrastructure (GI) and open spaces. Large and small spaces can contribute to cooling, with effects propagating up to approximately half the park's width due to street geometry (Hathway and Sharples, 2012; Upmanis et al., 1998). Street trees can offset anthropogenic heat from vehicles. Surfaces with high solar reflectance (albedo) choices can lead to reduced solar absorption and, thus, colder surfaces and lower temperatures in adjacent areas (Berisha, 2023; Oliveira et al., 2011; Taha, 1997). The term GI describes carefully organised networks of natural and semi-natural spaces intended to have positive effects on the environment, society, and economy. It has components that support biodiversity, water management, and climate mitigation, such as parks, green roofs, street trees, and urban forests (European Commission, 2019). With a focus on its cooling and pollution-filtering UHI and enhancing air quality. With an emphasis on cooling and air purification, GI provides quick, workable solutions that have a direct influence on public health and urban liveability, in contrast to more general Nature-Based Solutions (NbS), which can call for major land-use changes. The focus on GI in this study offers a distinctive addition to urban climate adaptation, emphasising how well it works to reduce air pollution and UHI.

Recent research has demonstrated the role of tree canopy cover in moderating UHI impacts. Ziter et al. (2019) found that even little green city spaces can dramatically reduce temperatures. Their findings showed that areas with significant tree canopy cover had temperature reductions of up to 4 °C compared to non-vegetated areas. Studies on high-albedo surfaces have also gained popularity. Mourales-Inzunza et al. (2023) investigated using reflective materials in urban planning. They discovered that surfaces with a high albedo can reduce surface temperatures by reflecting more sunlight. This method has proven beneficial when combined with vegetative cooling, indicating that integrated strategies produce the best results.

The mitigating effect of GI has been tested throughout the world, namely in Italy (Semenzato and Bortolini, 2023), Lisbon (Oliveira et al., 2011), London (Doick et al., 2014) and China (Ke et al., 2021). A recent review from Aram et al. (2019a,b) and an editorial by Aram et al. (2022) demonstrate that the cooling effect of GI is influenced by multiple factors, specifically that large urban parks with an area exceeding 10 ha tend to exhibit the most significant cooling effect in terms of both distance and intensity.

However, many urban areas suffer from insufficient GI, especially in the socioeconomically disadvantaged neighborhood (Hoffimann et al., 2017; Mears et al., 2019; Vidal et al., 2021). This deprivation exacerbates the UHI effect, leading to higher temperatures and increased health risks for vulnerable populations. Addressing the gaps in GI provision is crucial for reducing environmental inequalities and improving overall urban livability (Astell-Burt et al., 2014; Hoffimann et al., 2017; Jennings et al., 2017; Vidal et al., 2021; Shih, 2022). Individuals residing in areas more vulnerable face a heightened risk of experiencing adverse health effects due to increased temperatures, which can exacerbate existing social inequalities (Alves et al., 2023; Hsu et al., 2021; Vidal et al., 2022b). The prolongation of these inequalities or environmental injustice is exacerbated by limited access to air conditioning, inadequate housing conditions, and limited green open spaces, which further amplify the vulnerability of these populations to heat-related health risks.

In addition, urban spaces are also exposed to air pollution exacerbated by elevated temperatures caused by UHI, which increases energy consumption for cooling and worsens air quality by promoting the production of ground-level ozone and other pollutants. The GI plays a crucial role in purifying the urban air by filtering and absorbing gases and capturing harmful particles (Aram et al., 2019). As cities grow and urbanisation accelerates, deliberate installation and maintenance of GI become more critical in tackling the interrelated concerns of UHI and air pollution (Tara et al., 2015). Road traffic and industrial activities are typical anthropogenic sources of air pollutants in cities. Emissions from mobile sources contribute to both primary and secondary air pollution, pose risks to human health, harm ecosystems, and impact climate (Fonseca et al., 2023; Silva et al., 2012; Silva, 2015). According to estimates by the European Environment Agency, around 400.000 premature deaths can be attributed to air pollution each year in the EU, and 12,5% are related to nitrogen dioxide (EEA, 2019). The annual average concentration of NO_2 in Portugal has been particularly concerning in three air quality zones ('Lisboa Norte,' 'Porto Litoral,' and 'Entre Douro e Minho'), exceeding legal limits. Air pollution from nitrogen dioxide in these air quality zones primarily results from road traffic, especially diesel vehicles. Han et al. (2024) show that the GI system can decrease the UHI level and mitigate particulate matter issues in winter.

This study is motivated by the following research question: To what extent can the enhancement of GI coverage and connectivity reduce the intensity of UHI and mitigate urban air pollution in Porto, Portugal? The premise behind this issue is that increasing GI in cities results in notable drops in air pollution and UHI intensity, benefitting public health and urban liveability. The following are the study's goals.

- to evaluate Porto GI coverage and connectivity, as well as its connection to air pollution and UHI;
- to use empirical data to measure the effect of GI on reducing air pollution and mitigating UHI;
- to suggest urban planning techniques that improve GI in regions most impacted by air pollution and UHI, with an emphasis on neighbourhoods that are socioeconomically underprivileged.

The paper uses a case study of Porto, Portugal, to illustrate that limited GI fails to provide the cooling benefits required to alleviate UHI and does not contribute to mitigating air pollution. Porto's particular geographical and climatic context offers an excellent example of how urbanisation, if not managed with a focus on GI, can have negative environmental and public health consequences. This link between GI deprivation and UHI, and between GI deprivation and air pollution, emphasises the critical need for urban planning initiatives that prioritise the creation and management of green open spaces to improve urban liveability and environmental health. This study endeavors to address a

critical knowledge gap concerning the identification of the relationship between GI coverage, connectivity, and their interaction with UHI and air pollution.

The paper proceeds with the study area description and research methodology following this brief introduction. Subsequently, the UHI analysis results are based on meteorological sensor data, and the deprivation of GI is presented. The discussion and key research conclusions are presented after analysing the relationship between the UHI and green open spaces.

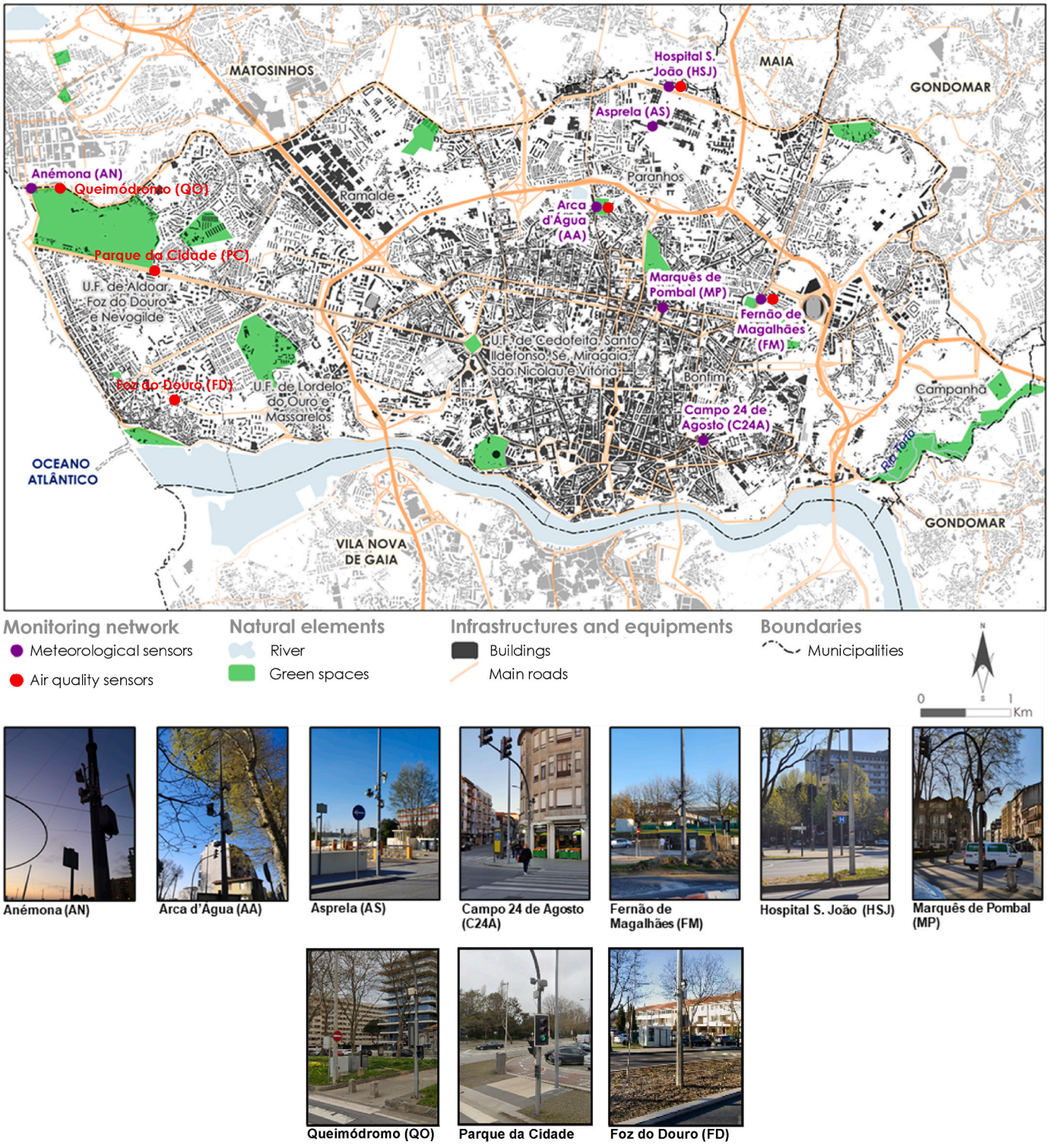


Fig. 1. Location of the Porto City Council climate monitoring network.
Note: Photographs were captured by the authors on March 23, 2021.
Source: Own elaboration.

2. Methodology

2.1. Study area

The study was conducted in Porto, a city northwest of mainland Portugal, covering an area of 41.42 km^2 and forming an integral part of the Porto Metropolitan Area (PMA). It is the core of the second most populous Portuguese metropolitan area, home to approximately 1,736,491 residents. It is closely behind the Lisbon Metropolitan Area, with 2,870,770 inhabitants (INE, 2021).

Geographically, Porto benefits from its strategic location along the coastline, bordered by the Atlantic Ocean to the west and the Douro River to the south. The city's gradual incline towards the ocean results in an elevation of 160 m, providing a picturesque backdrop (Gomes and Teixeira, 2020; Lopes et al., 2022a).

The study area boasts a temperate maritime climate, with average temperatures between 15 °C and 25 °C. Although occasional summer temperatures can peak at 35 °C, the winters are generally characterised by rainfall and cooler temperatures, fluctuating between 5 °C and 14 °C. According to the Köppen-Geiger climate classification system, Porto falls under the Csb category (Lopes et al., 2021, 2022b).

These climatic conditions assume significance in the context of urban discomfort during the summer, amplified by Urban Heat Island (UHI) effects and occasionally compounded by extreme heatwave occurrences. Interestingly, UHI effects in winter may contribute positively by potentially reducing energy consumption for heating purposes (Alcoforado, 2012).

2.2. Procedures

2.2.1. Monitoring network analysis

We use the data from a monitoring network managed by the Porto Digital company, installed by the Porto Municipal Council in 2019. The network includes 7 probes for Air Temperature (AT - °C)/Relative Humidity (RH - %) (Fig. 1), is part of the Smart Meteo Sense weather sensor network, associated with the UrbanSense platform, which is part of the European Future Cities project. The air quality in Porto has been assessed using the same platform, and it was possible to identify 6 air quality sensors distributed in the city. The devices are installed on public lighting poles at a height of 3.5 m, allocated within radiation protection shields, and their placement follows the guidelines from ISO 7726. It should be noted that the distribution of the monitoring network is not evenly spread throughout the territory, with significant gaps in essential areas of Porto municipality, such as industrial areas (e.g., Ramalde industrial area), leisure and recreation areas (e.g., Avenida dos Aliados, Rua de Santa Catarina, Rua das Flores), and green spaces and public gardens (e.g., Jardins do Palácio de Cristal and Jardim da Cordoaria).

In the municipality of Porto, the climate monitoring network represents several distinct morphoclimatic and urban occupancy contexts (see Appendix I). The monitoring stations were strategically selected to capture a diverse range of microclimatic conditions across Porto, from coastal influences at Foz do Douro and the Queimódromo to densely urbanised areas like Campo 24 de Agosto and Marquês de Pombal. This selection ensures comprehensive coverage of different urban typologies, allowing for a thorough analysis of the impact of various environmental and urban factors on local microclimates. A brief description of each sensor is summarised in Table 1.

The records of air temperature (AT) and relative humidity (RH – %) were taken every 15 min, and data analysis was performed for hourly averages. If the data had errors or failures, it was excluded from the analysis and deleted from the database. After processing the provided data (organising, correcting, and restructuring the database), data selection was made for hourly analysis during the winter (December, January and February – DJF) and summer (June, July and August – JJA) climatological periods between 2019 and 2022. Anomalies in the schedules were checked against the other sensors and Portuguese

Table 1
Description of the sensors used in the monitoring network.

Name		Description of the sensor
Anémona	AN	Located in the western part of the city, exposed to the north and under the influence of western ocean breezes, characterized by the coexistence of a built-up area to the north (the residential area of Matosinhos) and bordered to the east by the city's main green area – Porto's City Park.
Arca d'Água	AA	Located near the expansive spaces of the Arca d'Água Garden, in a low-density built environment, associated with residential areas.
Asprela	AS	It is inherent to the main knowledge and business know-how transfer hub in the city of Porto; there are nearby significant number of faculties of the University of Porto and prestigious private universities (e.g., Portucalense University); since 2018, this area has been undergoing transformation, endowing it with a green area (the city's "green lung") for the enjoyment of those who work or study daily at the Asprela campus.
Campo 24 de Agosto/ Ferreira Cardoso	C24A	Associated with the presence of a square located in the Bonfim parish; with high urban density and low to medium-rise buildings, it is close to one of the main bus terminals and several neighborhood-scale supermarkets (e.g., Continente Bom Dia); it is a highly urbanised area.
Fernão de Magalhães/ Monte Aventino	FM	An area near the Dragão Stadium and Antas, associated with one of the urban expansion areas of recent decades, where a significant residential area and some of the essential services for the daily life of Porto residents (e.g., the Citizen's Shop) are visible; the weather sensor is located near Dr. Francisco Sá Carneiro Garden, but due to the high urban density and its location in the central area of one of the city's most important roadways, it experiences reduced influence from the green space.
Foz do Douro	FD	Foz do Douro represents one of the most emblematic areas of Porto, situated at the confluence of the Douro River and the Atlantic Ocean. The area is renowned for its coastal landscape, beaches and maritime environment. The buildings are characterized by a low-rise profile, with a preponderance of residential functions. The monitoring station in Foz do Douro is situated in an area where the influence of the ocean is predominant, providing distinctive climatic conditions, including the pervasive presence of sea breezes and a lower temperature variation compared to other more inland areas of the city.
Hospital S. João	HSJ	Located in the northern part of the city, away from the influence of the Douro River, and one of the stations most exposed to the northern winds (predominant in summer), situated in a high-rise built environment that confers high aerodynamic roughness; in this area, there are several interstitial spaces free of construction, although the trend is towards infill; besides being one of the main residential areas of Porto, it is also associated with the location of the reference hospital for the northern region of mainland Portugal – the Hospital of S. João
Marquês de Pombal/ Constituição	MP	An area of confluence of the parishes of Santo Ildefonso, Bonfim, and Paranhos, associated with the presence of a densely wooded square, which is highly sought after on hot days, especially by elderly individuals; there are some points of interest in this area, namely the Pedro Ivo Popular Library and the Church of Senhora da Conceição.
Parque da Cidade	PAC	Porto City Park is the largest urban park in Portugal, covering an area of approximately 83 ha. Located in the western part of the city, the

(continued on next page)

Table 1 (*continued*)

Name		Description of the sensor
		park extends to the Atlantic coast, allowing for a direct interaction between the green spaces and the influence of the sea. The monitoring station in the City Park is essential for studying the effects of large green areas in environmental conditions.
Queimódromo	QUE	The Queimódromo, situated near the City Park and the Foz do Douro coastal zone, constitutes a vast open expanse that is frequently utilized for outdoor gatherings such as the *Queima das Fitas*, which attracts a considerable number of individuals on an annual basis. The monitoring station situated within this area captures data from a zone that encompasses both the direct influence of the ocean and extensive open spaces devoid of substantial vegetation, thereby providing an intriguing contrast to measurements obtained in more wooded or densely urbanised regions.

Source: Own elaboration.

Institute for Sea and Atmosphere (IPMA) data to check the recorded data. After eliminating errors or failures recorded in the system at a given time, data for 219 winter days and 245 summer days were considered due to omissions or errors in at least one of the sensors. The Air Urban Heat Island (UHI_{air}) Intensity was calculated for each hourly record in the available series between Porto-Pedras Rubras (Airport station) and the set of sensors distributed throughout the city of Porto, considering daytime and nighttime periods for both summer and winter stations.

UHI_{air} intensity in Porto represents the difference between the observed AT at each sensor station in the CMP network and the recorded AT at the Airport station, followed by intra-urban differentiation. To understand the intra-urban temperature changes during the day, it calculates the UHI_{air} intensity for each hour. This calculation uses Equation (1)to create a time series.

$$UHIair = ATurb(h) - ATsub\ (h)$$

Urban Air Temperature (AT_{urb} – h) refers to the mean hourly air temperature observed in each urban site of the Porto Digital network, and Suburban Air Temperature (AT_{sub} - h) is the mean hourly air temperature observed at the Airport station. Analyses were grouped by summer (JJA) and winter (DJF) climatological season, with specific time periods within a month and a day, to identify trends among different sensors and assess the impact of increased AT at different locations.

The resulting time series were subjected to empirical distribution analysis, where representative hourly percentiles were calculated to evaluate the daily profiles of UHI_{air} intensity at each location, including the median (UHI_{air}50p) and the lower/upper extremes of the $25^{th}$and 75^{th}quartiles (UHI_{air}25p and UHI_{air}75p, respectively). The daily cycle of UHI_{air} was also classified into different stages based on the sign (positive versus negative) and slope of the hourly UHI_{air} variation rate.

This study also uses data from air quality sensors for selected pollutants, which may vary according to source type or data availability. The current paper presents the pollutants considered in urban areas, all of which typically result from road traffic, namely CO (Carbon Monoxide), NO_2 (Nitrogen Dioxide), $PM_{2.5}$ (Particulate matter <2.5 μm), PM_{10} (Particulate matter <10 μm), and O_3 (Ozone).

Pollutant concentration records were collected at 15-min intervals, and data analysis was performed to calculate annual averages. After data processing, which included organising, correcting, and restructuring the database, data were selected for annual analysis from 2019 to 2022.

2.2.2. Heat risk index (HRI), green infrastructure and deprivation

The Heat Risk Index (HRI) was assessed through a comprehensive spatial analysis that integrated vital parameters, including land surface temperature (LST), land cover classification, and demographic data. A remote sensing approach was employed to capture and process high-resolution satellite imagery, deriving land surface temperature gradients across the study area. This index was designed to provide a holistic representation of the vulnerability landscape, highlighting areas with heightened susceptibility to heat-related health risks within the urban fabric.

The HRI was formulated by integrating hazard, exposure, and vulnerability domains. These indicators were normalised and weighted using the Analytic Hierarchy Process (AHP) method, following a 55% weight for hazard, 35% for exposure, and 15% for vulnerability. Data in all variables and indices was classified using the quantile method, categorising them into five risk classes. Comparative weights were determined based on an AHP process of pairwise comparison (Estoque et al., 2020). Five academic and professional experts in the thematic were asked about the weights to be assigned. The assigned values are within various other studies (e.g., Estoque et al., 2020). The aggregation of indicators and the use of weights was in line with the IPCC recommendations on the derivation of vulnerability indices, namely that "a climate vulnerability index is typically derived by combining, with or without weighting, several indicators assumed to represent vulnerability" (IPCC, 2014: 1775).

This study used the LST for the hazard component. These data were acquired from LANDSAT 8-OLI imagery covering the summer months (June, July, and August) between 2013 and 2022, with a maximum cloud cover of 10%. Utilising the infrared band 10 (10.30–11.30 μm), LST values were derived with a spatial resolution of 100 m, subsequently resampled to 30 m using the cubic convolution resampling method. These LST values were determined inversely using Planck's Law, as described by Weng (2009). The scenes were processed using the Global Estimate of Surface Temperature repository (Parastatidis et al., 2017), and gaps caused by cloud cover were filled using a 9 × 9 matrix moving average.

Meteorological data, including Air Temperature (AT), Wind Speed (WS), Wind Direction, Atmospheric Pressure, and Relative Humidity for 12 days, were acquired from IPMA's data for the Porto reference station (Pedras Rubras) and metadata archives. Based on these procedures, the identification of Urban Heat Island (UHI) areas was established based on Ma et al.'s method (2010), using Equation (2) to define the limits of the regions exposed to UHI.

$$LST > \mu LST + (0,5 \times \sigma LST) \quad (2)$$

Where LST is the Land Surface Temperature, μLST is the mean of the Land Surface Temperature, and σLST is the standard deviation of the Land Surface Temperature.

Table 2 shows the meteorological conditions of the extracting scenes.

Additionally, the Environmental Criticality Index (ECI) was computed by combining LST and Normalised Difference Vegetation Index (NDVI) values (Ranagalage et al., 2017; Senanayake et al., 2013), where both values were stretched to enhance clarity and contrast. This process was critical to avoid infinite values resulting from NDVI equating to 0, adhering to Senanayake et al. method (2013). It uses the following Equation (3):

$$NDVI = \frac{[d(band\ 5) - d(band\ 4)]}{[d(band\ 5) + d(band\ 4)} \quad (2)$$

where d corresponds to the digital number (DN) of bands 4 and 5 of the Landsat 8-OLI image.

The LST and NDVI values were extended using the histogram equalisation method for pixel values between 1 and 255 to improve the contrast and clarity resulting from the original layer and to avoid infinite values of the ECI resulting from the presence of NDVI values equal to 0 (Senanayake et al., 2013). The ECI was obtained using the following Equation (3):

Table 2
Summary of weather conditions related to LANDSAT 8 - OLI satellite scenes.

Date	Hour (a.m. – GMT +00)	Solar Azimute	Solar Elevation	Air Temperature (AT) (°C)	Wind Speed (WS) ($km.h^{-1}$)	Wind Direction	Pressure (hPa)	Relative Humidity (RH – %)
04/06/2013	11:15:55	132.33	65.99	26	13	ESE	1 004.26	34
20/06/2013	11:15:47	129.42	66.27	16	19	NNW	1 013.18	68
09/07/2014	11:13:42	128.69	64.57	23	15	NNE	1 010.21	47
29/08/2015	11:13:39	144.37	54.23	23	9	NNE	1 007.23	78
14/07/2016	11:13:24	132.33	63.17	26	19	ENE	1 009.22	32
01/07/2017	11:13:38	128.09	65.33	19	19	NNE	1 018.14	52
02/08/2017	11:13:49	134.53	60.72	21	11	WNW	1 012.19	56
18/06/2018	11:12:23	131.42	65.17	29	11	NW	1 011.20	40
21/08/2018	11:12:56	143.09	55.34	26	9	W	1 006.24	57
25/07/2020	11:13:22	134.65	61.39	23	17	NW	1 008.58	73
28/07/2021	11:13:53	132.98	61.69	24	11	WNW	1 006.60	69
31/07/2022	11:14:16	136.32	60.38	29	11	W	1 006.60	61

Source: Own elaboration.

$$ECI_{(LST-Veg)} = \frac{LST(stretched\ 1-255)}{NDVI(stretched\ 1-255)} \quad (3)$$

LST (stretched 1–255) refers to the extended values of the LST, while NDVI (stretched 1–255) corresponds to the widening of the values of the NDVI pixels. Five classes were defined using the quantile classification method (very low, low, moderate, high and very high). Although the water bodies produce the lowest NDVI values, they do not represent environmentally critical areas and, therefore, had to be excluded from the analysis (Senanayake et al., 2013).

Exposure was quantified using population density as an indicator of heat exposure. This approach aligns with previous studies (Morabito et al., 2015; Tomlinson et al., 2011), calculated consistently with the Hazard Index. The overall heat exposure index for each area was determined, considering the population and area of each census tract.

The vulnerability assessment encompassed sensitivity and adaptive capacity factors. Sensitivity factors included population demographics (age distribution and socioeconomic structure) and building characteristics extracted from the 2021 census. Adaptive capacity was based on variables related to GI, shelter areas, health services, and literacy levels of the resident population.

The GI mapping was conducted through a systematic surveying process that involved identifying and categorising various vegetation elements within the study area. High-resolution aerial imagery was analysed using Geographic Information System (GIS) tools to delineate and quantify the spatial distribution of GI, including parks, trees, and other vegetation covers.

The GI data were obtained by analysing the satellite images and the corresponding NDVI between 2013 and 2022. For this purpose, the Fractional Vegetation Cover (FVC) was calculated. The FVC was calculated using the formulation proposed by Carlson et al. (1995) (Eq. (4)):

$$FVC = (NDVI^*)^2 \quad (4)$$

where FVC is the per cent vegetation and NDVI* is the normalised NDVI. FVC translates the percentage of vegetation at ground level in each census tract area based on its vertical projection (Yang et al., 2016). FVC = 0 has no vegetation, and FVC = 100 has dense vegetation. All indicators (see Appendix II) have been combined to allow the analysis of hazard exposure-vulnerability following the HRI proposal proposed by Lopes et al. (2023).

Furthermore, ground truthing exercises were carried out to validate the accuracy of the mapped GI elements. The collected data were then integrated into the GIS platform to generate a GI map, illustrating the availability and distribution of vegetation components within the urban environment.

The HRI and GI analysis integration involved overlaying the spatial datasets generated from the respective assessments. This process facilitated the identification of areas exhibiting a disparity between heightened heat vulnerability and the presence or absence of GI elements. The quantitative analysis of this integrated dataset enabled the identification of correlations between the distribution of GI and the spatial patterns of heat stress.

Fig. 2 summarises the flowchart of the integrated methodology for measuring the relationship between HRI, air pollution, and green space deprivation.

2.2.3. Statistics analysis

Main descriptive analysis and statistical tests were performed. In this sense, the statistical analysis software SPSS (Statistical Package for the Social Sciences), version 29.0 was used. The Kruskal-Wallis test was conducted to assess differences in sensor measurements across locations during distinct seasonal and temporal periods. Significant p-values indicate statistically significant differences in measurements between sensor locations.

3. Results

3.1. Urban heat island analysis

Local climatic-meteorological conditions were investigated based on a monitoring network established by the Porto City Council in 2019. Despite the limitations inherent in the geographical distribution of sensors and the time period of the measured data, we can infer from the AT which areas in the municipality of Porto are more or less sensitive to UHI_{air}. UHI_{air} intensity in Porto reflects the difference between the observed temperature at each station in the CMP sensor network and the temperature recorded at the Airport station. The intensity of UHI_{air} in Porto exhibits a well-defined daily rhythm. Fig. 3 summarises the

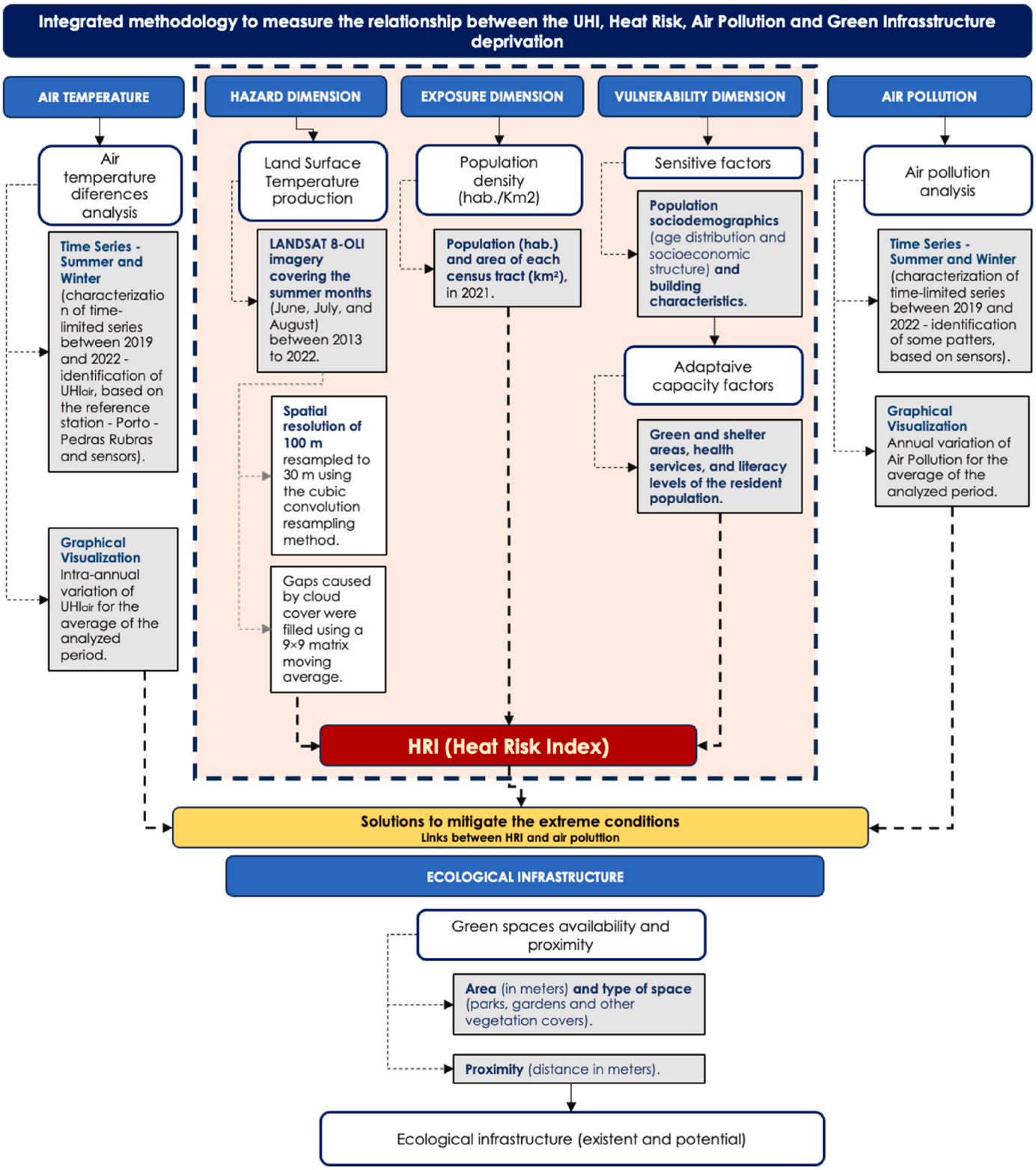


Fig. 2. Flowchart of integrated methodology to measure the relationship between the Urban Heat Island (UHI), Heat Risk Index (HRI), air pollution and Green Infrastructure (GI) deprivation. Source: Own elaboration.

conditions during the summer and winter periods between 2019 and 2022 for the seven climate monitoring sensors, representative of distinct morphoclimatic characteristics and land use and occupancy in Porto.

When analysing the relationships between sensors using the Kruskal-Wallis test, significant differences in UH_{Iair} intensity were observed among most monitoring locations during summer and winter, as summarised in Table 3. For instance, Anémona (AN) consistently exhibited significant differences ($p < .001$) when compared to all other sensors during sunset and night periods across seasons. In contrast, Marquês de Pombal (MP) showed notable differences with most sensors, particularly during winter sunset and night periods, suggesting higher variability in densely urbanised areas.

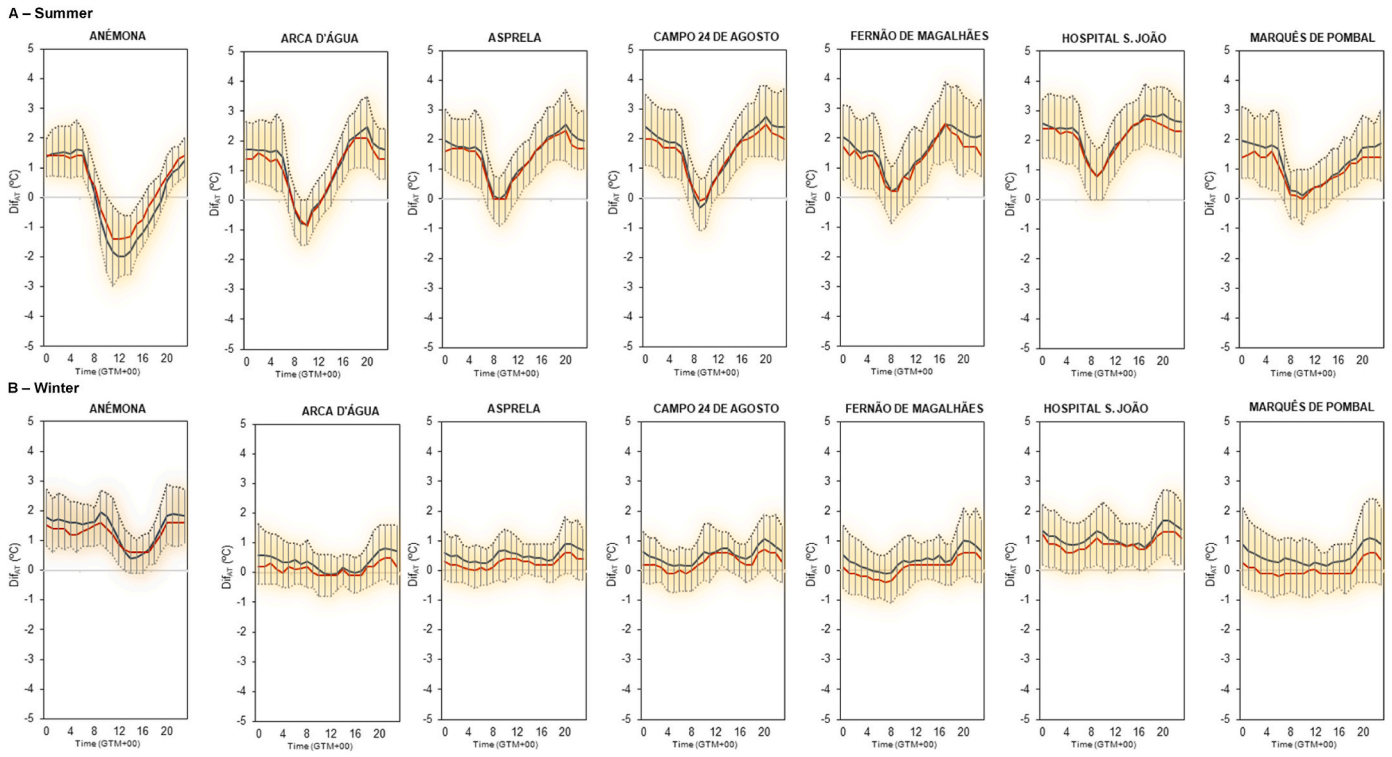


Fig. 3. Daily cycle of the intensity of the UHI (Dif_{AT} between the sensor and Reference Station) observed in the municipality of Porto, between 2019 and 2022, and by climatological season of the year – Summer (JJA) (A) and Winter (DJF) (B): average, median ($UHI_{air}50p$), first quartile ($UHI_{air}25Q$) and third quartile ($UHI_{air}75Q$). Source: Own elaboration, based on data from Porto Digital Association–CMP.

Table 3
Spatial analysis of the Urban Heat Island (UHI) in different sensors in summer and winter seasons (sunset and night).

Sensor	Comparison (p-value) – Kruskal-Wallis Test			
	Summer (sunset)	Summer (night)	Winter (sunset)	Winter (night)
Anémona (AN)	AA (<.001); AS (<.001); C24A (<.001); FM (<.001); HSJ (<.001); MP (<.001)	AA (<.05); AS (<.001); C24A (<.001); FM (<.001); HSJ (<.001); MP (<.001)	AA (<.001); AS (<.001); C24A (<.001); FM (<.001); HSJ (<.001); MP (<.001)	AA (<.001); AS (<.001); C24A (<.001); FM (<.001); HSJ (<.001); MP (<.001)
Arca d'Água (AA)	AN (<.001); MP (<.001)	AN (<.001); AS (<.001); C24A (<.001); HSJ (<.001)	AN (<.001); AS (.002); C24A (<.001); FM (.006) HSJ (<.001); MP (<.001)	AN (<.001); FM (<.001); HSJ (<.001); MP (.023)
Asprela (AS)	AN (<.001); MP (<.001)	AN (<.001); AA (<.001); MP (<.001)	AN (.002); AA (.002); C24A (<.001); HSJ (.007)	AN (<.001); HSJ (<.001); MP (<.001)
Campo 24 de Agosto (C24A)	AN (<.001); MP (<.001)	AN (<.001); AA (<.001); FM (<.001); MP (<.001)	AN (<.001); AA (<.001); AS (.001); FM (.001)	AN (<.001); FM (<.001); HSJ (<.001)
Fernão de Magalhães (FM)	AN (<.001); MP (<.001)	AN (<.001); AS (<.001); C24A (<.001); HSJ (<.001); HSJ (<.001)	AN (<.001); AA (<.006); C24A (<.001); HSJ (.006)	AN (<.001); AA (<.001); C24A (<.001); HSJ (<.001); MP (<.001)
Hospital de São João (HSJ)	AN (<.001); MP (<.001)	AN (<.001); AA (<.001); FM (<.001); MP (<.001)	AN (<.001); AA (<.001); AS (.007); FM (.006)	AN (<.001); AA (<.001); AS (<.001); C24A (<.001); FM (<.001); MP (<.001)
Marquês de Pombal (MP)	AN (<.001); AA (<.001); AS (<.001); C24A (<.001); FM (<.001); HSJ (<.001)	AN (<.001); AS (<.001); C24A (<.001); HSJ (<.001)	AN (<.001); AA (<.001); C24A (.001); HSJ (.006)	AN (<.001); AA (.023); AS (<.001); FM (<.001); HSJ (<.001);

Source: Own elaboration.

When it comes to the seasonality of UHI_{air} intensity, there is a broader range of values during the summer, both between the curves of the 75th quartile (Q_{75}) and the 25th quartile (Q_{25}), and between the daily maximums and minimums of the mean and median ($UHI_{air}P_{50}$) (Fig. 4). This indicates higher variability and intensity. As anticipated, due to its western location near the beach and morning fog, the Anémona station experiences an extended period of lower summer temperatures than the Airport. Analysing the daily profiles of various urban sensors facilitates identifying the UHI_{air} intensity cycle, which can be classified into the following periods (Fig. 3).

(1) Higher UHI_{air} intensity occurs in the late afternoon during the summer in most sensors (Arca d'Água, Asprela, Campo 24 de Agosto/Ferreira Cardoso, Fernão de Magalhães/Monte Aventino, and Hospital de S. João), except for Anémona where it remains stable until dawn. Kruskal-Wallis test results support these observations, showing significant differences in UHI_{air} intensity between Anémona and other sensors during sunset ($p < .001$) and night ($p < .05$). Summer intensities are higher than winter, particularly in densely populated urban areas, ranging from brief occurrences in Arca d'Água, Asprela, and Campo 24 de Agosto to

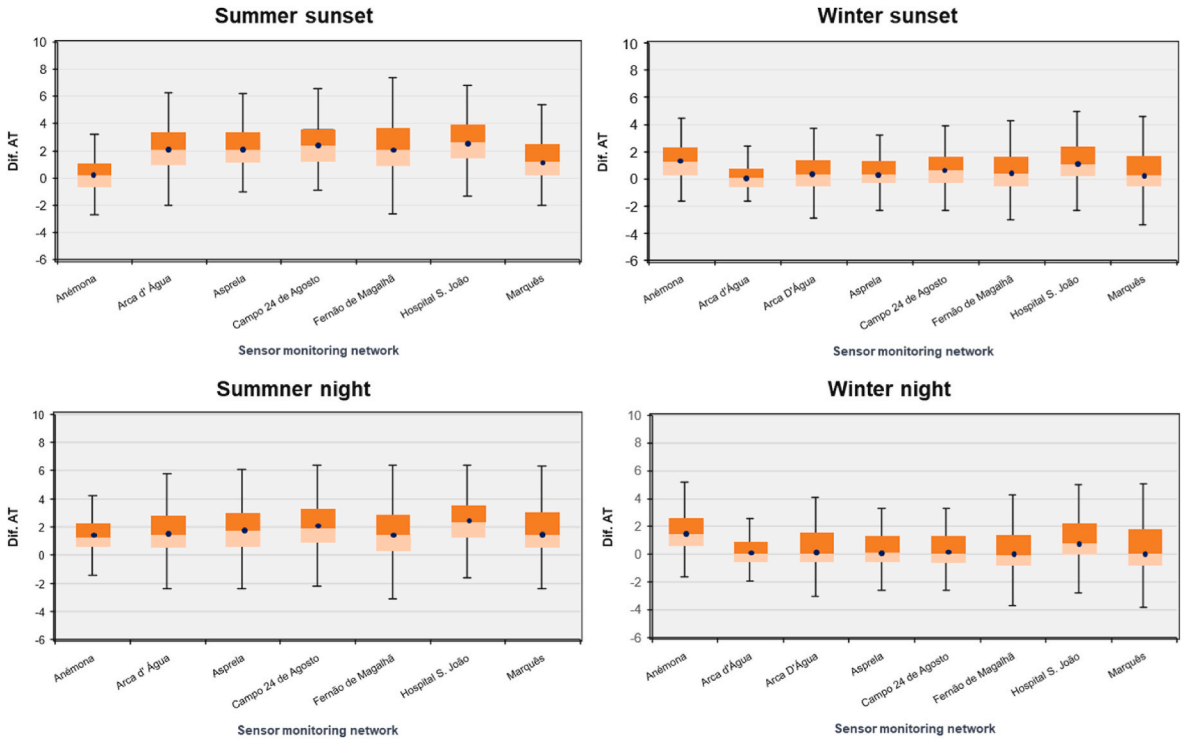


Fig. 4. Diagrams of extremes and quartiles of the intensity of the UHI in summer (JJA) and winter (DJF) (sunset - 18:00 GMT+00 to 20:59 GMT+00 and night - 21:00 GMT+00 to 06:59 GMT+00) in the sensors of the Porto monitoring network.
Source: Own elaboration, based on data from Porto Digital Association – CMP.

more prolonged periods in Anémona, peaking at 5 a.m. in summer and 7 a.m. in winter.

(2) UHI_{air} intensity decreases during twilight.

(3) UHI_{air} intensity remains stable during the night in both summer and winter, characterised by more minor differences between quartile curves and minimal variations (mainly decreases below 0.1 °C per hour).

(4) Negative average and median UHI_{air} intensity are observed in the morning, with urban areas colder than the reference Airport station. In summer, this period is more stable, lasting 2–4 h in most monitoring sensors (Arca d'Água, Asprela, Campo 24 de Agosto, Fernão de Magalhães). However, Anémona experiences over 8 h of lower AT compared to the Airport and Hospital de S. João, differing from the 2019–2022 period. Kruskal-Wallis analysis confirms significant morning differences, especially between Anémona and densely urbanised locations such as Marquês de Pombal ($p < .001$). This behaviour extends to other sensors during winter (e.g., Anémona and Asprela). The Marquês de Pombal sensor exhibits higher average UHI_{air} intensity (>1.0 °C) between 3:00 p.m. GMT+00 and 3:00 a.m. GMT+00 in winter.

(5) UHI_{air} intensity increases daily, with a more rapid temperature difference than the Airport during the summer. The hourly variation in UHI_{air} intensity is lower during winter. In contrast, more substantial average variations are observed in densely populated and consolidated urban areas (e.g., Campo 24 de Agosto/Ferreira Cardoso, Fernão de Magalhães/Monte Aventino, Hospital de S. João, and Marquês de Pombal), confirmed by the significant p-values in the Kruskal-Wallis tests across seasons.

The profiles of mean and median UHI_{air} intensity (P_{50}) throughout the day reveal similar temporal patterns across locations. However, the analysis of summer and winter seasons provides additional evidence by elucidating the disparities among sensors that are more sensitive to specific seasonal conditions. Particularly noteworthy is that Marquês de Pombal exhibited identical UHI_{air} intensity values (median of intensity peak and median of stable nighttime period) for both summer and winter during the 2019–2022 period. On the other hand, Campo 24 de Agosto/Ferreira Cardoso, Fernão de Magalhães/Monte Aventino, and Hospital de S. João consistently displayed the highest daytime UHI_{air}.

3.2. *Heat risk index and existing green infrastructure*

Areas with higher heat anomalies also showed increased vulnerability and limited adaptive capacity. Heat stress exhibited a decreasing spatial trend from the primary urban area towards the bordering coastal and eastern regions (Fig. 5). The effect of the green spaces of Parque da Cidade and Serralves also manage to minimize the effects of heat stress (with a very low HRI classification). The most intense danger related to extreme heat was predominantly observed in parishes affected by the Urban Heat Island (UHI), particularly U.F. de Cedofeita, Santo Ildefonso, Sé, Miragaia, São Nicolau e Vitória (79.4%), Bonfim (76.8%), and Paranhos (71.5%).

The vulnerability was less intense in the city edge blocks. In contrast, the statistical subsections of the city centre showed a high to very high vulnerability index. The lowest vulnerability indices were correlated with areas characterised by younger, wealthier populations, newly constructed areas, abundant GI, and improved natural ventilation conditions.

The spatial analysis of human exposure highlighted a limited population density range across Porto, emphasising a pattern of urban solid pressure. Population density decreased from the city centre towards the surrounding areas. The most significant exposure values were concentrated in distinct areas with different sociodemographic characteristics.

32.6% of Porto's territory is in areas with a high Heat Risk Index (HRI). The parish of Bonfim presents the largest territorial area susceptible to risk, with 41.4% of the parish exhibiting a very high HRI. Regions deserving particular attention are those situated in areas of high to very high HRI, primarily housing a more vulnerable elderly

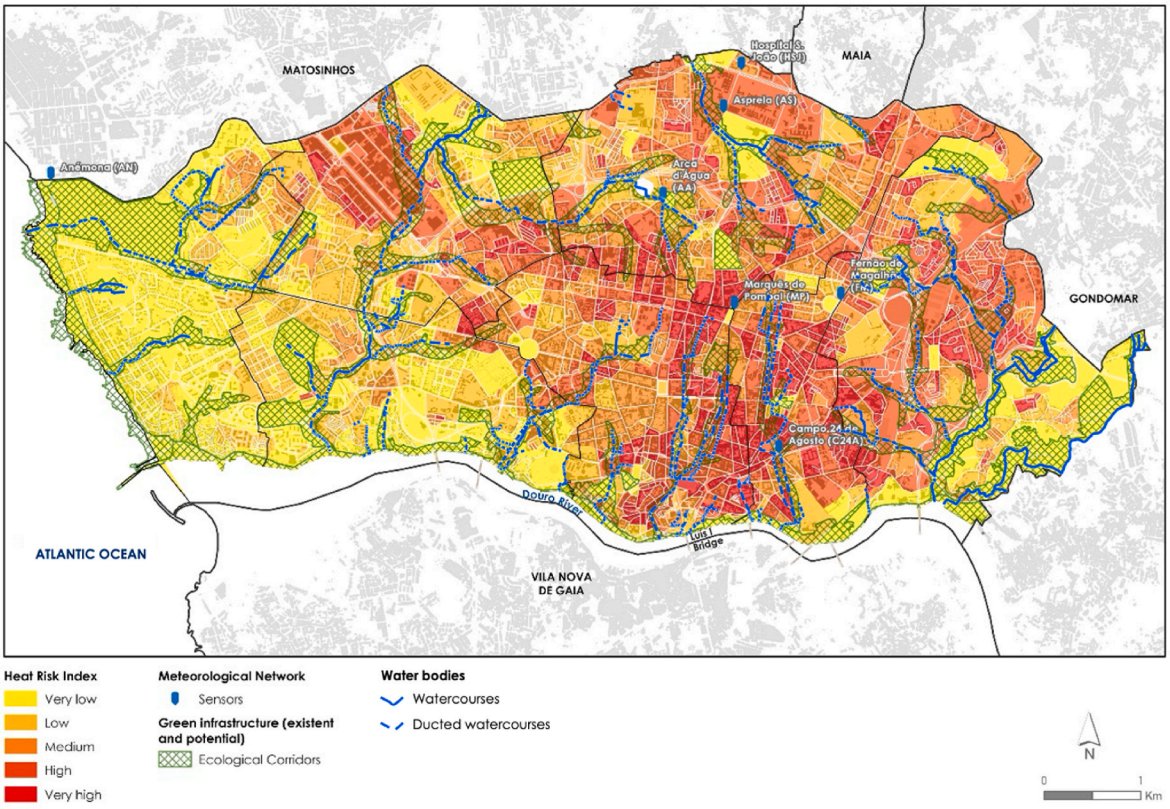


Fig. 5. Heat Risk Index (HRI), Green infrastructure (potential and existing) and distribution of meteorological network in the municipality of Porto. Source: Authors' own elaboration.

population.

The combined map (Fig. 5) delineates a complex vulnerability landscape, revealing concentrated pockets of heightened heat risk within Porto's central and eastern regions. This vulnerability hotspot coincides with an observable deficiency in GI, accentuating the interdependence between GI and vulnerability to heat-related health risks. This spatial distribution of heightened vulnerability also signals the potential health risks associated with prolonged exposure to elevated temperatures in these densely populated urban zones. Furthermore, the map elucidates the nuanced influence of the surrounding natural water bodies, hinting at their potential to attenuate vulnerability gradients and foster localised resilience through passive cooling mechanisms. The evident scarcity of GI within the vulnerable zones reflects a systemic oversight that exacerbates the disproportionate exposure of marginalised communities to the adverse impacts of heat stress. It is also crucial to acknowledge that a substantial proportion of the response to the challenges posed by extreme heat risk hinges on strategically exploiting the existing and potential ecological corridors within the municipality (see Fig. 5).

Results from the analysis of the UHI_{air} dynamics in Porto corroborate the findings presented in the combined map analysis. The confirmation of UHI_{air} intensity as a prevalent phenomenon, particularly during the evening and night periods, resonates with the depicted concentration of heightened heat risk in Porto's central and eastern sectors during the same timeframes. Furthermore, the indication of elevated UHI_{air} intensity during the summer aligns with the visual representation of a broader range of heat risk values during the same season, emphasising the amplified vulnerability and intensity experienced during the warmer months. The variability and intensity documented in the UHI_{air} profiles echo the observed scarcity of GI in vulnerable urban zones, substantiating the crucial role of vegetation in mitigating the adverse impacts of intensified heat stress.

The distinctive UHI_{air} intensity cycles identified within the daily profiles further underline the critical influence of local environmental factors, such as coastal proximity and GI, in shaping the temporal variability of heat stress in Porto. This temporal correspondence stresses the interconnected nature of urban vulnerability dynamics. It highlights the potential of strategic GI integration as a viable approach to modulate the intensity and duration of the UHI_{air} effect.

3.3. *Air pollution and existing green infrastructure*

The preliminary air quality analysis provides valuable comprehension into trends and variations in pollutant concentrations over the years.

Their temporal distribution is shown in Fig. 6. The pollutants are divided into two types: primary and secondary. As a primary pollutant, CO has a decreasing average value, falling from 0.4 mg/m^3 in 2019 to 0.12 mg/m^3 in 2021 and 0.23 mg/m^3 in 2022. For each year, approximately 25% of the data falls in the first quartile (Q_1), 50% in the median, and 25% in the third quartile (Q_3). The same variation was observed in the NO_2 plot, with a decreasing mean value from 51.27 μg/m^3 in 2019 to 32.37 μg/m^3 in 2022. This evolution is accompanied by a significant dispersion around the median of each year, including a marked increase in the interquartile range from 34.7 μg/m^3 in 2019 to 17.25 μg/m^3 in 2022. Statistical analysis using the Kruskal-Wallis test revealed highly significant differences in NO_2 concentrations between all years, particularly between 2019 and subsequent years ($p < .001$). The sharp decline in 2021 aligns with reduced anthropogenic emissions during the COVID-19 lockdown, as highlighted by the adjusted test results.

However, as a secondary pollutant, the median value for O_3 increased from 34.25 μg/m^3 in 2019 to 44 in 2022, indicating an increasing trend over time. The box plot shows that the Q_1 and the third quartile (Q_3) are increasing, indicating a high dispersion of the data. The

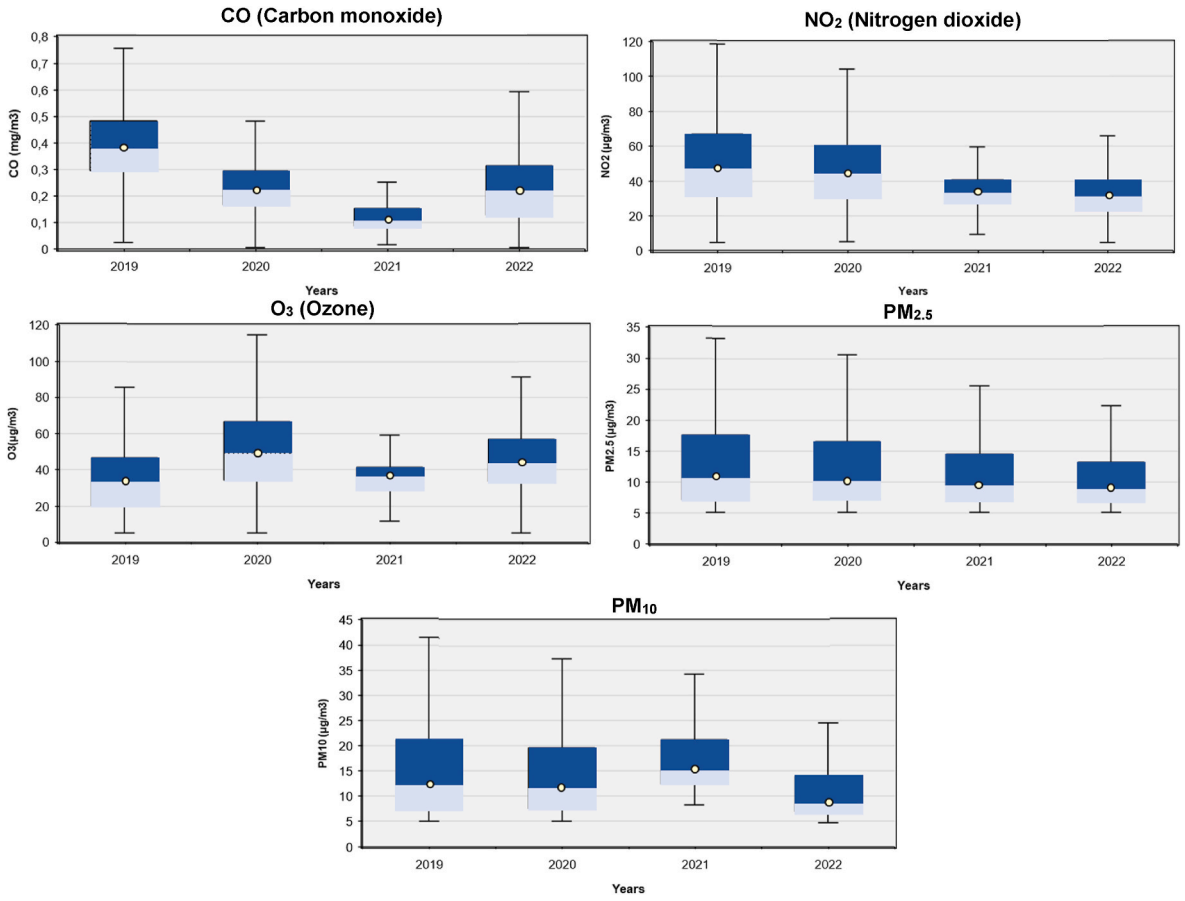


Fig. 6. Diagrams of extremes and quartiles of different air pollutant during different years. Quartiles (Q25 and Q75) and Median (50% of the sample) were considered.
Source: Own elaboration, based on data from Porto Digital Association–CMP.

lines extending beyond the box indicate the data range. The range in 2022 is from 5 µg/m^3 to 91.25 µg/m^3, indicating a high diversity. The maximum values are scattered, indicating the presence of outliers, especially in 2020 and 2022. This distribution could be caused by the relatively high average annual temperature of 2020 (15.9 °C) compared to the other years. The Kruskal-Wallis test confirmed significant differences in O_3 levels across all years ($p < .001$).

PM's ($PM_{2.5}$ - particulate matter <2.5 µm and, PM_{10} - particulate matter <10 µm), is a mixture of solid and liquid particles suspended in the air, including dust, soot, smoke, and aerosols. These pollutants can interact with gases, influencing processes such as atmospheric chemical reactions, particularly involving compounds like NOx, SO_2, and VOC (volatile organic compounds). For PM_{10}, the mean concentration varies over the years, from 17.33 µg/m^3 in 2019 to 11.46 µg/m^3 in 2022. The values of the Q_1 and the third quartile (Q_3) show a different degree of dispersion, with an interquartile range (IQR) that widens from 13.65 µg/m^3 in 2019 to 7 µg/m^3 in 2022. The whiskers in the boxplot show a wide range of attention, with the highest values in 2019 and 2020. There has been a general decline in $PM_{2.5}$ concentration over time, as evidenced by the mean concentration falling from 14.98 µg/m^3 in 2019 to 11,09 µg/m^3 in 2022. The interquartile range (IQR) for the Q_1 and Q_3 decreases from 10,43 µg/m^3 in 2019 to 6,23 µg/m^3 in 2022, indicating a declining trend in their respective values. The box plot whiskers show a wide range of concentrations with high maximum values, especially in 2019 and 2020. The mean concentration is typically higher than the median each year, indicating a positively skewed distribution. In particular, 33,22 µg/m^3 is the upper limit for 2019. Kruskal-Wallis test results also confirmed statistically significant differences in $PM_{2.5}$ levels across all years ($p < .001$). These findings underline the general improvement in PM2.5 levels, likely attributed to stricter regulations and reduced traffic emissions.

The decrease in concentrations of primary pollutants such as CO and NO_2 in 2021 due to the COVID-19-related lockdown highlights the direct influence of human activities on the emissions of these pollutants. However, the increase in O_3 concentrations and variations in particle concentrations (PM10 and $PM_{2.5}$) suggest the presence of other factors, such as meteorological and seasonal conditions, that may play a crucial role in air quality. It is also worth mentioning the important role of NO2 as a precursor to O_3 and its contribution to the formation of secondary PM.

When evaluating air quality data at different monitoring stations, patterns that may be related to or determine the UHI can be seen during the summer and winter season (Fig. 7). Arca D'Água sensor, located in an area with high traffic flow, showed significant concentrations of PM_{10} in winter 2019, with 14.0 µg/m^3. The fact that the City Park is located close to the Leixões seaport area and near a major traffic route may indicate its influence. It should be noted, for example, that the sea breeze can carry atmospheric pollutants or contribute to the aeration and renewal of the air. The presence of fine particles, such as $PM_{2.5}$, can be influenced by factors such as air salinity and the presence of marine aerosols, as well as exhaust emissions from the combustion of fossil fuels.

Therefore, when analysing $PM_{2.5}$ and PM_{10} concentrations in Parque da Cidade, it is advisable to consider the local geography and environmental characteristics, including proximity to coastal areas. A more in-depth analysis, considering the prevailing wind direction (namely the influence of NW winds), specific weather patterns and the local topography, can improve the perception of the possible influence of beach

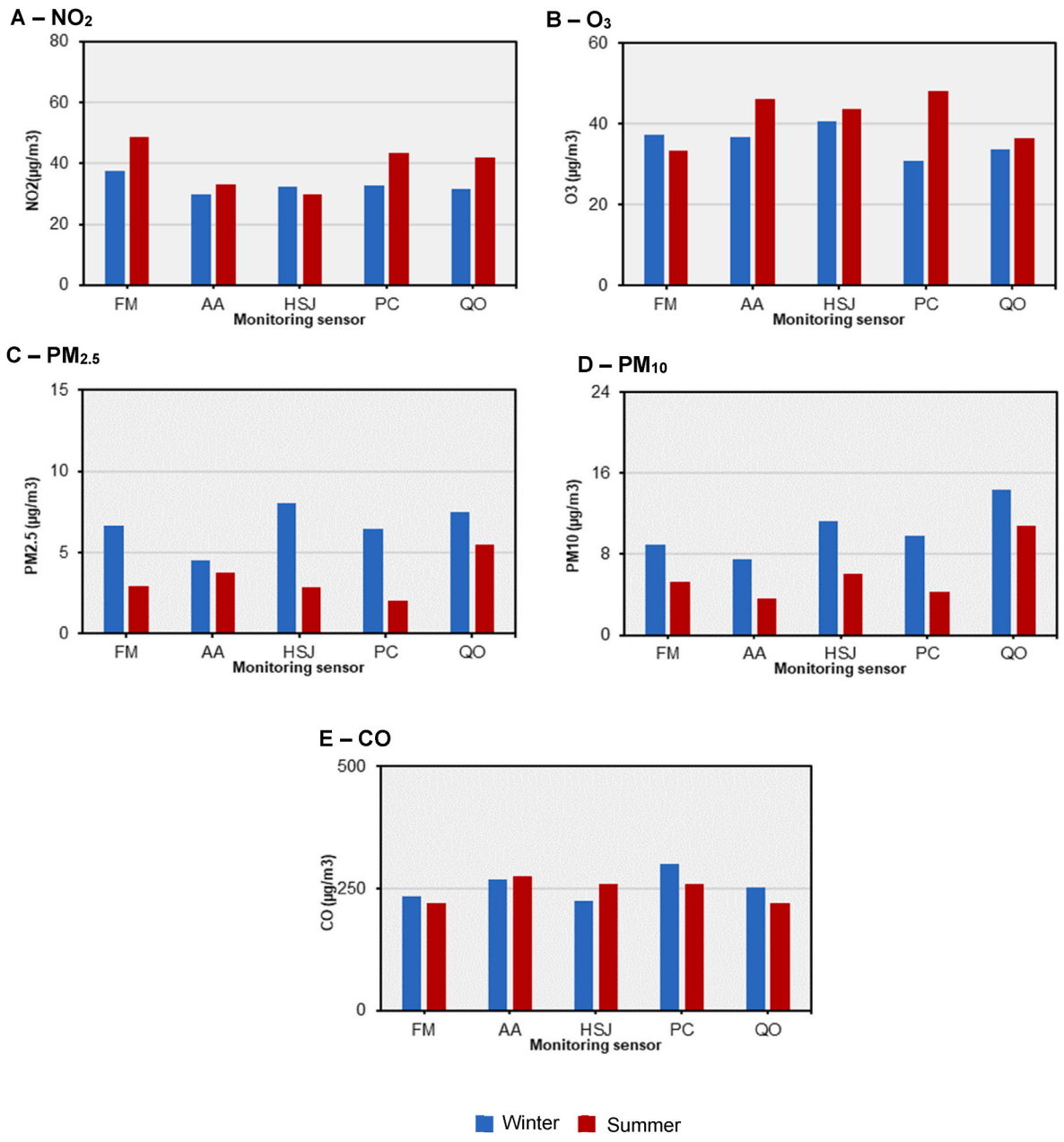


Fig. 7. Analysis of different air pollutant by season mean (4-year – 2019–2022). (A) NO_2; (B) O_3; (C) $PM_{2.5}$; (D) PM_{10}; (E) CO.
Note: FM – Fernão de Magalhães; AA – Arca d'Água; HSJ – Hospital S. João; PC – Parque da Cidade; QO – Queimódromo.
Source: Own elaboration, based on data from Porto Digital Association–CMP.

areas on pollutant concentrations in this geographical area.

Significant variations between the various years indicate the influence of seasonal and meteorological factors on air quality. The comparison between winter and summer data reinforces the possibility of UHI effects, especially its influence during summer.

4. Discussion

At the end of the 19th century, more than 75% of Porto's territory was covered by green areas. However, 100 years later, these areas have decreased to less than 30%, a reduction of approximately 60% due to urbanisation. This transformation has led to phenomena such as the UHI effect, increased stormwater runoff, reduced groundwater recharge, altered soil properties, and changes in biodiversity patterns. These reflect the significant impact of human activities and the replacement of predominantly permeable areas with built surfaces, further fragmenting and disrupting ecosystems (Alberti, 2008; Pauleit and Breuste, 2011). Although this tendency is in line with European urbanisation trends, Porto's depletion of green space and its effects should be compared to those of other large European cities. The loss of green space in Porto reflects larger patterns seen in 19th- and 20th-century European cities as a result of population development and industrialisation. But compared to cities like Vienna and Berlin, which adopted more proactive urban planning techniques to conserve green spaces, Porto's reduction—60% over a century—is especially striking (Vidal et al., 2021). Due to careful urban design and conservation efforts like the Vienna Woods, Vienna maintains more than 50% green or agricultural space, acting as a counterbalance to Porto. This coordinated strategy has improved stormwater management, bolstered biodiversity, and reduced the severity of UHI. Vienna is a prime example of how proactive measures can strike a balance between ecological sustainability and urban growth (Brenner et al., 2021). With green areas making up around 40% of the

city, Berlin exemplifies a more comprehensive approach to urban greening (Kabisch et al., 2016a,b). Many of the problems that cities like Porto face have been lessened by past conservation initiatives, such as the preservation of wooded areas. The advantages of integrating green infrastructure into urban development are demonstrated by Berlin's improved stormwater management and comparatively low UHI intensity. Intriguingly, the spatial disparity between vulnerability hotspots and the distribution of GI serves as a stark visual manifestation of the underlying environmental injustice previously identified by several authors (Graça et al., 2018; Hoffimann et al., 2017; Vidal et al., 2021; Lopes et al., 2023).

Similar to other international cities, the UHI effect in Porto shows a positive relationship with air temperature intensity during heatwave events (Santamouris, 2015). Figs. 3 and 4 illustrate this UHI pattern across all sensors during summer, highlighting a distinct daily temperature cycle between urban and rural areas. This cycle includes a diurnal UCI around solar noon, a nocturnal UHI from night to morning, and two rapid transition periods. These results are consistent with studies conducted in different geographical locations (e.g., Basara et al., 2008; Camilloni and Barrucand, 2012; Oliveira et al., 2021). This correspondence aligns with the documented impacts of UHI on local microclimates, reflecting the pronounced susceptibility of densely populated urban zones to heightened heat stress (Monteiro, 1997; Monteiro et al., 2018). Reinforcing the conclusions of previous studies on UHI_{air} in Porto (Monteiro, 1997; Monteiro et al., 2018), and in line with other reference literature (Oke, 1982, 1987; Oke et al., 2017), we are pleased to highlight the consistency of the data in at least 50.0% of the frequencies. Thus, UHI_{air} intensity is a positive phenomenon, especially during the evening and night, regardless of the urban location or season.

The profiles of UHI_{air} intensity throughout the day demonstrate analogous temporal patterns across locations, thereby substantiating the findings of prior studies in other cities. These prior studies indicated that the influence of urban land use is consistent in producing comparable results among sensors (e.g., Nantes, Angers, and La Roche-sur-Yon, in France) (Bernard et al., 2017) and Lisbon (Oliveira et al., 2021).

In Porto, 32.6% of the territory is in areas with a high heat risk index (HRI). Bonfim is the most affected parish (41.4% very high HRI). The city encompasses a diverse array of GI scattered across its densely woven urban landscape. These GI exhibit a wide variety of characteristics, including variations in age, size, usage, spatial attributes, surroundings, and vegetation cover and structure (Farinha-Marques et al., 2014). A report on the ecological framework and biodiversity of the city of Farinha-Marques et al. (2018), as part of the ongoing review of the Porto Municipal Master Plan (PDM), revealed that the total area of green urban spaces in the city amounts to 13.0 km^2, representing approximately 31.4% of the municipality's area. Consequently, there is approximately 54.8 m^2 of green space per inhabitant in Porto, surpassing the desirable value for the urban green structure – 50 m^2/hab -, advocated by World Health Organization (2010).

However, this does not mean complete coverage, as certain areas still lack sufficient GI, which are crucial to mitigating urbanisation's adverse effects (Hami et al., 2019). Norton et al. (2015) analysed the relationship between the size of green spaces and their effectiveness in cooling urban areas, utilising Melbourne as a case study. The study's findings supported the hypothesis that larger parks have a more pronounced cooling effect, influencing urban planning policies to favour the creation of more extensive or contiguous GI. The cooling effect can be enhanced through evapotranspiration by larger green areas with extensive vegetation, improving the capacity to absorb pollutants.

A study by Dimoudi & and Nikolopoulou (2003) in Athens supports our observation that urban morphology plays a critical role in the effectiveness of GI. While many studies, such as those by Tzoulas et al. (2007), suggest limited benefits of green spaces in highly dense urban areas, our research found that even in dense urban environments, green spaces can be highly effective if strategically placed and well-maintained. This difference may be due to the specific urban characteristics or the methodologies used in these studies, highlighting the importance of considering local context in urban greening strategies. For example, a 2023 review by McDonald et al., (2023) looked at how to reconcile green investments with urban density. The study challenges the idea that high density and significant green space are mutually exclusive by indicating that these goals can be accomplished in cities through deliberate planning. Furthermore, a spatially explicit model to evaluate the impact of urbanisation on ecosystem services was presented (van Oorschot et al., 2024), highlighting the significance of taking urban morphology into account when planning for green infrastructure (GI) and stresses how optimising the placement of grey and green infrastructure can improve urban sustainability.

The municipality of Porto continues to have areas potentially exposed to air pollution, particularly in the northern sector, which also experiences a higher intensity of the UHI_{air} effect. It is crucial to highlight that the persistence of air pollution hotspots can impact air quality and contribute to the intensity and magnitude of the UHI phenomenon. The UHI can affect local temperature, wind patterns, and air quality. Reducing atmospheric pollutant concentrations can modify the LST by diminishing surface solar radiation through scattering and absorption (Yang et al., 2016). While elevated particulate matter concentrations have been associated with rises in LST (Jin et al., 2010). However, they can concurrently increase and decrease in both LST. This duality is attributed to the augmented scattering of shortwave radiation and entrapment of longwave radiation, as indicated in studies by Li et al. (2018); Song et al. (2018). Neighbourhoods with higher GI density not only have lower concentrations of pollutants like NO_2 and PM_{10} but also experience better overall air quality. The HRI analysis supports the recommendation that GI and water points should be refuges during extreme temperatures, providing critical relief from heat stress. The analysis and mapping of the HRI prompt the formulation of specific recommendations to guide people during extreme temperature occurrences, directing them away from high-risk locations. GI and water points within the city emerge as suggested havens during hot days, providing respite from heat stress and offering public safety and comfort avenues.

Long-term mitigation options include cooling city roofs by transforming them into "green" roofs incorporating vegetation that contributes to temperature reduction. Existing academic literature underscores the multi-faceted benefits of green solutions in urban settings for addressing climate change and improving residents' health and well-being by reducing air pollution (Colding et al., 2006; Kabisch et al., 2016a,b; Livesley et al., 2016). As climate uncertainties loom on the horizon, this approach not only serves as a shield against immediate health risks but also fortifies the very fabric of urban society, equipping it to weather the storms of an unpredictable future (Andreucci et al., 2021; Lencastre et al., 2023). In Porto, several initiatives have been undertaken to address the deficiency of green areas, including efforts to increase the number of trees in streets and urban parks. For example, 3484 trees were planted in 2024, adding more than 67,000 trees to the city's grove. Over the past 10 years, 77 ha have been improved or expanded, including 22 ha of new green space. Currently, 30 ha of new green spaces are under construction or planned. In addition, the Asprela Central Park will be inaugurated in 2022, protecting people, goods and infrastructure such as the metro line (Porto City Council, 2024). Despite these initiatives, certain urban requalification and construction interventions may inadvertently contribute to the emergence of new risk areas.

Central studies consider the UHI phenomena, atmospheric pollutant concentrations (NO_2, CO, O_3, PM_{10}, $PM_{2.5}$) and changes in urban areas cover are significantly correlated (Hidalgo-García and Arco-Díaz, 2023; Hu et al., 2020; Shafizadeh-Moghadam et al., 2020; Tomlinson et al., 2011). We can also find possible associations in this study area according to the preliminary analysis. Although the results are still experimental, it is possible to hypothesise that air pollution may have significant impacts on the local population's quality of life, directly

affecting their exposure to unfavourable atmospheric conditions, as suggested by other studies (Hidalgo-García and Arco-Díaz, 2023; Kelly and Fussell, 2015; MacKerron and Mourato, 2009).

Given the preliminary nature of this study, it is advisable to conduct more in-depth analyses, considering additional factors such as prevailing wind direction, specific weather patterns and local topography. This more holistic approach may provide a more complete understanding of the region's air pollution patterns and the potential effects of the UHI. For example, in Xi'An (China), Han et al. (2024) found that the GI system would significantly increase the summer ozone level. This observation was not yet possible to verify in our study. The persistence of high levels of air pollution can be a significant concern for public health and the quality of life of local populations, underscoring the importance of effective mitigation strategies and environmental policies (Chen et al., 2023; Eckelman and Sherman, 2016; Hidalgo-García and Arco-Díaz, 2023).

5. Conclusions

This study demonstrates that enhancing coverage and connectivity of GI in urban environments can contribute to the reduction of air pollution levels. This paradigm shift, steered by a nature-centric urban planning approach, embodies a proactive stride toward cultivating cities that can adeptly navigate the complexities of the rapidly changing climate (Chiesura, 2004; Lencastre et al., 2023; Meadowcroft, 2009; Vidal et al., 2022a). The synergistic interplay between the spatial vulnerability gradient and the embracing presence of natural water bodies, such as the Douro River and the Atlantic Ocean, unveils a tapestry of possibilities for holistic climate adaptation strategies, harnessing the intrinsic resilience embedded within natural ecosystems (Cai et al., 2018; Wu and Zhang, 2019; Zhu et al., 2022).

GI is essential for improving air quality because of their impact on local air circulation, noise reduction, and biodiversity promotion. To fully realise the benefits of GI in mitigating air pollution, however, regular evaluations and focused pollution control measures are required due to the possibility of outliers and variability in air pollutant levels.

Based on the results, it is essential to provide specific recommendations for policymakers and practitioners. For this context, some examples of implemented strategies are as follows.

1) *To prioritise the development of large and connected green spaces.* Considering the reduction mentioned above and the need to enhance specific areas of Porto that lack green spaces and have higher levels of pollution and UHI, such as in the northern part of the municipality, the need for intervention becomes clear. In some cases, their placement is difficult. However, the use of vertical vegetation and rooftop gardens is an excellent example of how green spaces can be effectively integrated into dense urban environments.
2) *To promote the use of native and drought-resistant plants.* In Portugal, several trees are listed as well adapted to the local climate and recognised for their role in reducing the UHI or filtering pollutants (see FAPAS guide, Trees in Portugal and Europe – Humphries and Sutton, 2005). Their consideration for ornamental purposes is essential in the municipality of Porto.
3) *To incorporate the GI in urban planning.* Policymakers should encourage the integration of GI, such as green roofs, green walls and permeable pavements, in new developments and retrofit projects. In this context, the municipality of Porto has been working to valorise the planting of trees by individuals and the placement of trees in some streets. The municipality's latest inventory is concerned with verifying the needs and operational results of tree planting in Porto's streets assessing their role in thermal comfort.
4) *To establish an Urban Heat Island Action Plan.* This plan should align with Portugal's long-term climate change goals and the targets outlined in the Paris Agreement. Such an initiative would address the immediate challenges posed by urban heat islands and contribute to broader climate resilience and sustainability objectives, ensuring cohesive and forward-looking urban planning strategies.
5) *To engage the community in greening initiatives,* such as designing, implementing, and maintaining green spaces. The enrolment can foster a sense of ownership and ensure that these spaces meet the needs of residents.

6. Limitations and future studies

The research has some limitations that need to be considered in future studies. The spatial and temporal distribution of the monitoring network, established by the City Council of Porto in 2019, has some gaps in some geographical areas with specific attributes or characteristics. Data gaps and inequalities occur due to the uneven distribution of the monitoring network, especially in critical areas such as industrial zones and recreational areas. The main limitations of this study are related to data constraints. Several sites have incomplete time series, resulting in temporal discontinuities that reduce the availability of synchronous air temperature measurements. This results in fewer days with complete hourly data for all sensors. In addition, there are no readily available data sets for local wind currents other than those from Porto Airport.

External factors, such as COVID-19 closures, can distort air quality trends. Also, limited air quality sensor coverage may not capture the complexity of pollutant interactions in certain areas.

On the other hand, GI assessments directly correlate with reduced heat risk. However, they can be influenced by maintenance and vegetation health factors. The research suggests more in-depth team analyses considering prevailing wind direction, weather patterns, and local topography to fully understand the interactions between air quality, urban heat, and vulnerability. It would be essential to consider whether we had a complete basis for wind direction analysis in the Porto Digital database. In other studies, we could estimate important variables for future parameter measurements through simulation. The purely numerical nature of this study prevents us from assessing other subjective dimensions that may be present in the study area, which could be explored using qualitative analysis methods such as questionnaire surveys, focus groups, or workshops. It will also be essential to evaluate the effects of the interventions carried out by the City Council in the medium and long term, estimating the effects on the attenuation of the UHI and the reduction of air pollution from anthropogenic sources.

CRediT authorship contribution statement

Hélder Silva Lopes: Writing – review & editing, Writing – original draft, Visualization, Validation, Supervision, Software, Resources, Project administration, Methodology, Investigation, Funding acquisition, Formal analysis, Data curation, Conceptualization. **Diogo Guedes Vidal:** Writing – review & editing, Writing – original draft, Visualization, Formal analysis. **Nadhima Cherif:** Writing – original draft, Formal analysis. **Lígia Silva:** Writing – review & editing, Writing – original draft, Visualization. **Paula C. Remoaldo:** Writing – review & editing, Investigation, Funding acquisition.

Declaration of competing interest

The authors declare that they have no known competing financial interests or personal relationships that could have appeared to influence the work reported in this paper.

Acknowledgments

This publication was supported by the Multiannual Funding of the Laboratory of Landscapes, Heritage and Territory (Lab2PT), Ref. UIP/04509/2020, financed by national funds (PIDDAC) through FCT/Q3 MCTES.

Appendix A. Supplementary data

Supplementary data to this article can be found online at https://doi.org/10.1016/j.jenvman.2025.124446.

Data availability

Data will be made available on request.

References

Alberti, M., 2008. Urban patterns and ecosystem function. In: Alberti, M. (Ed.), Advances in Urban Ecology. Springer, Boston, pp. 61–92. https://doi.org/10.1007/978-0-387-75510-6_3.

Alcoforado, M.J., 2012. Planning procedures towards high climatic quality cities. Example referring to Lisbon. Finisterra 41. https://doi.org/10.18055/finis1449.

Alves, F., Leal, C., Vidal, D.G., 2023. Promover Territórios Resilientes e Saudáveis num Clima em Mudança: Impactos das Alterações Climáticas na Saúde Humana numa Região Vulnerável do Sul da Europa. RECIMA21 - Rev. Científica Multidiscip. https://doi.org/10.47820/recima21.v4i10.4180. ISSN 2675-6218 4, e4104180.

Andreucci, M.B., Loder, A., Brown, M., Brajković, J., 2021. Exploring challenges and opportunities of biophilic urban design: evidence from research and experimentation. Sustain. Times 13, 4323. https://doi.org/10.3390/su13084323.

Aram, F., García, E.H., Solgi, E., Mansournia, S., 2019a. Urban green space cooling effect in cities. Heliyon 5 (4), e01339. https://doi.org/10.1016/j.heliyon.2019.e01339.

Aram, F., Higueras García, E., Solgi, E., Mansournia, S., 2019b. Urban green space cooling effect in cities. Heliyon 5, e01339. https://doi.org/10.1016/j.heliyon.2019.e01339.

Aram, F., Shahab, S., Solgi, E., 2022. Editorial: impacts of urban green spaces on environmental perceptions and social life. Front. Environ. Sci. 10. https://doi.org/10.3389/fenvs.2022.1050597.

Arunab, K.S., Mathew, A., 2024. Quantifying urban heat island and pollutant nexus: a novel geospatial approach. Sustain. Cities Soc. 101, 105117. https://doi.org/10.1016/j.scs.2023.10511.

Astell-Burt, T., Feng, X., Mavoa, S., Badland, H.M., Giles-Corti, B., 2014. Do low-income neighbourhoods have the least green space? A cross-sectional study of Australia's most populous cities. BMC Public Health 14. https://doi.org/10.1186/1471-2458-14-292.

Basara, J.B., Hall Jr, P., Schroeder, A.J., Illston, B.G., Nemunaitis, K.L., 2008. Diurnal cycle of the Oklahoma City urban heat island. J. Geophys. Res. 113, D20109. https://doi.org/10.1029/2008JD010311.

Berisha, A., 2023. Solar and human activity impact on high and low land river flows. Civ. Eng. J. 9 (7). https://doi.org/10.28991/CEJ-2023-09-07-06.

Bernard, J., Musy, M., Calmet, I., Bocher, E., Kéravec, P., 2017. Urban heat island temporal and spatial variations: empirical modeling from geographical and meteorological data. Build. Environ. 125, 423–438. https://doi.org/10.1016/j.buildenv.2017.08.009.

Brenner, A.-K., Mocca, E., Friesenecker, M., 2021. Vienna's urban green space planning. In: Kazepov, Y., Verwiebe, R. (Eds.), Vienna: Still a Just City? Routledge, pp. 117–130. https://doi.org/10.4324/9781003133827-12.

Cai, Z., Han, G., Chen, M., 2018. Do water bodies play an important role in the relationship between urban form and land surface temperature? Sustain. Cities Soc. 39, 487–498. https://doi.org/10.1016/j.scs.2018.02.033.

Camilloni, I., Barrucand, M., 2012. Temporal variability of the Buenos Aires, Argentina, urban heat island. Theor. Appl. Climatol. 107, 47–58. https://doi.org/10.1007/s00704-011-0459-z.

Carlson, T.N., Gillies, R.R., Schmugge, T.J., 1995. An interpretation of methodologies for indirect measurement of soil water content. Agric. For. Meteorol. 77, 191–205. https://doi.org/10.1016/0168-1923(95)02261-U.

Cetin, M., 2019. The effect of urban planning on urban formations determining bioclimatic comfort area's effect using satellitia imagines on air quality: a case study of Bursa city. Air Qual. Atmos. Health 12, 1237–1249. https://doi.org/10.1007/s11869-019-00742-4.

Chen, A., Zhao, X., Yao, L., Chen, L., 2016. Application of a new integrated landscape index to predict potential urban heat islands. Ecol. Indic. 69, 828–835. https://doi.org/10.1016/j.ecolind.2016.05.045.

Chen, X.H., Tee, K., Elnahass, M., Ahmed, R., 2023. Assessing the environmental impacts of renewable energy sources: a case study on air pollution and carbon emissions in China. J. Environ. Manag. 345, 118525. https://doi.org/10.1016/j.jenvman.2023.118525.

Chiesura, A., 2004. The role of urban parks for the sustainable city. Landsc. Urban Plann. 68, 129–138. https://doi.org/10.1016/j.landurbplan.2003.08.003.

Cichowicz, R., Bochenek, A.D., 2024. Assessing the effects of urban heat islands and air pollution on human quality of life. Anthropocene, 100433. https://doi.org/10.1016/j.ancene.2024.100433.

Colding, J., Lundberg, J., Folke, C., 2006. Incorporating green-area user groups in urban ecosystem management. Ambio 35, 237–244. https://doi.org/10.1579/05-A-098R.1.

Dang, T.T., Oanh, T.T.K., Thanh, H.L., Nguyen, T.N., 2023. Impacts of foreign direct investment on economic development: does institutional quality matter? Econ. Sociol. J. 7 (6). https://doi.org/10.28991/ESJ-2023-07-06-05.

Dimoudi, A., Nikolopoulou, M., 2003. Vegetation in the urban environment: microclimatic analysis and benefits. Energy Build. 35 (1), 69–76. https://doi.org/10.1016/S0378-7788(02)00081-6.

Doick, K.J., Hutchings, T.R., Lawrence, V., 2014. Keeping London a cool place to Be: the role of greenspace. In: Trees, People and the Build Environment II Conference. University of Birmingham, Birmingham, pp. 85–95.

Eckelman, M.J., Sherman, J., 2016. Environmental impacts of the U.S. health care system and effects on public health. PLoS One 11, e0157014. https://doi.org/10.1371/journal.pone.0157014.

EEA, 2019. Air Quality in Europe – 2019 Report (No. 10/2019). Publications Office of the European Union, Luxembourg.

European Commission, 2019. Commission Staff Working Document. Guidance on a Strategic Framework for Further Supporting the Deployment of EU-Level Green and Blue Infrastructure. EC, Brussels.

Falah, N., Karimi, A., Harandi, A.T., 2020. Urban growth modeling using cellular automata model and AHP (case study: qazvin city). Model. Earth Syst. Environ. 6, 235–248. https://doi.org/10.1007/s40808-019-00674-z.

Farinha-Marques, P., Alves, P.C., Fernandes, C.O., Guilherme, F., Gonçalves, C., 2018. Revisão do Plano Diretor Municipal do Porto - Suporte Biofísico e Ambiente. Estrutura Ecológica e Biodiversidade (Relatório de Caracterização e Diagnóstico). Porto.

Farinha-Marques, P., Fernandes, C., Lameiras, J., Leal, I., Silva, S., Guilherme, F., 2014. Morfologia e Biodiversidade nos Espaços Verdes da Cidade do Porto. Caderno 1 - Seleção das áreas de estudo, CIBIO-UP, Porto. 2a edição revista e aumentada, second ed. Faculty of Science of the University of Porto, Porto.

Fonseca, F., Paschoalino, M., Silva, L., 2023. Health and well-being benefits of outdoor and indoor vertical greening systems: a review. Sustain. Times 15, 4107. https://doi.org/10.3390/su15054107.

Giles-Corti, B., Lowe, M., Arundel, J., 2020. Achieving the SDGs: evaluating indicators to be used to benchmark and monitor progress towards creating healthy and sustainable cities. Health Pol. 124, 581–590. https://doi.org/10.1016/j.healthpol.2019.03.001.

Gomes, J., Teixeira, I., 2020. Geomorfologia. In: Fernandes, J.R. (Ed.), Geografia Do Porto. Book Cover, pp. 14–25. Porto.

Graça, M., Alves, P., Gonçalves, J., Nowak, D.J., Hoehn, R., Farinha-Marques, P., Cunha, M., 2018. Assessing how green space types affect ecosystem services delivery in Porto, Portugal. Landsc. Urban Plann. 170, 195–208. https://doi.org/10.1016/j.landurbplan.2017.10.007.

Hami, A., Abdi, B., Zarehaghi, D., Maulan, S.B., 2019. Assessing the thermal comfort effects of green spaces: a systematic review of methods, parameters, and plants' attributes. Sustain. Cities Soc. 49, 101634. https://doi.org/10.1016/j.scs.2019.101634.

Hathway, E.A., Sharples, S., 2012. The interaction of rivers and urban form in mitigating the Urban Heat Island effect: a UK case study. Build. Environ. 58, 14–22. https://doi.org/10.1016/j.buildenv.2012.06.013.

Hidalgo-García, D., Arco-Díaz, J., 2023. Spatiotemporal analysis of the surface urban heat island (SUHI), air pollution and disease pattern: an applied study on the city of Granada (Spain). Environ. Sci. Pollut. Res. 30, 57617–57637. https://doi.org/10.1007/s11356-023-26564-7.

Hoffimann, E., Barros, H., Ribeiro, A.I., 2017. Socioeconomic inequalities in green space quality and Accessibility—evidence from a Southern European city. Int. J. Environ. Res. Publ. Health. https://doi.org/10.3390/ijerph14080916.

Hsu, A., Sheriff, G., Chakraborty, T., Manya, D., 2021. Disproportionate exposure to urban heat island intensity across major US cities. Nat. Commun. 12. https://doi.org/10.1038/s41467-021-22799-5.

Hu, Y., Dai, Z., Guldmann, J.M., 2020. Modeling the impact of 2D/3D urban indicators on the urban heat island over different seasons: a boosted regression tree approach. J. Environ. Manag. 266, 110424. https://doi.org/10.1016/j.jenvman.2020.110424.

Humphries, C.J., Sutton, D.A., 2005. Guia FAPAS – Árvores de Portugal e Europa [Guide FAPAS – Trees of Portugal and Europe], second ed. Porto: Fundo para a Proteção dos Animais Selvagens e Planeta das Árvores (FAPAS).

INE, 2021. Censos 2021 [WWW Document]. URL. https://www.ine.pt/scripts/db_censos_2021.html, 3.25.22.

Jennings, V., Baptiste, A.K., Osborne Jelks, N., Skeete, R., 2017. Urban green space and the pursuit of health equity in parts of the United States. Int. J. Environ. Res. Publ. Health 14. https://doi.org/10.3390/ijerph14111432.

Jin, M., Shepherd, J.M., Zheng, W., 2010. Urban surface temperature reduction via the urban aerosol direct effect: a remote sensing and wrf model sensitivity study. Adv. Meteorol. 2010, 1–14. https://doi.org/10.1155/2010/681587.

Kabisch, N., Frantzeskaki, N., Pauleit, S., Naumann, S., Davis, M., Artmann, M., Haase, D., Knapp, S., Korn, H., Stadler, J., Zaunberger, K., Bonn, A., 2016a. Nature-based solutions to climate change mitigation and adaptation in urban areas: perspectives on indicators, knowledge gaps, barriers, and opportunities for action. Ecol. Soc. 21. https://doi.org/10.5751/ES-08373-210239.

Kabisch, N., Strohbach, M., Haase, D., Kronenberg, J., 2016b. Urban green space availability in European cities. Ecol. Indic. 70, 586–596. https://doi.org/10.1016/j.ecolind.2016.02.02.

Ke, X., Men, H., Zhou, T., Li, Z., Zhu, F., 2021. Variance of the impact of urban green space on the urban heat island effect among different urban functional zones: a case study in Wuhan. Urban For. Urban Green. 62. https://doi.org/10.1016/j.ufug.2021.127159.

Kelly, F.J., Fussell, J.C., 2015. Air pollution and public health: emerging hazards and improved understanding of risk. Environ. Geochem. Health 37, 631–649. https://doi.org/10.1007/s10653-015-9720-1.

Kim, S.W., Brown, R.D., 2021. Urban heat island (UHI) intensity and magnitude estimations: a systematic literature review. Sci. Total Environ. 779, 146389. https://doi.org/10.1016/j.scitotenv.2021.146389.
Lencastre, M.P.A., Vidal, D.G., Lopes, H.S., Curado, M.J., 2023. Biophilia in pieces: critical approach of a general concept. Environ. Soc. Psychol. 8, 1869. https://doi.org/10.54517/esp.v8i3.1869.
Li, H., Meier, F., Lee, X., Chakraborty, T., Liu, J., Schaap, M., Sodoudi, S., 2018. Interaction between urban heat island and urban pollution island during summer in Berlin. Sci. Total Environ. 636, 818–828. https://doi.org/10.1016/j.scitotenv.2018.04.254.
Livesley, S.J., McPherson, E.G., Calfapietra, C., 2016. The urban forest and ecosystem services: impacts on urban water, heat, and pollution cycles at the tree, street, and city scale. J. Environ. Qual. 45, 119–124. https://doi.org/10.2134/jeq2015.11.0567.
Lo, S.T., Chan, E.Y., Chan, G.W., Murray, V., Abrahams, J., Ardalan, A., Kayano, R., Yau, J.W., 2017. Health emergency and disaster risk management (Health-EDRM): developing the research field within the Sendai framework paradigm. Int. J. Disaster Risk Sci. 8, 145–149. https://doi.org/10.1007/s13753-017-0122-0.
Lopes, H., Remoaldo, P., Ribeiro, V., Martín-Vide, J., 2023. In: Leal Filho, W., Vidal, D.G., Dinis, M.A.P. (Eds.), The Impacts of Climate Change on Human Well-Being in the Municipality of Porto—An Analysis Based on Remote Sensing. Climate Change Management. Springer, Cham, pp. 135–172. https://doi.org/10.1007/978-3-031-26592-1_8.
Lopes, H.S., Remoaldo, P.C., Ribeiro, V., Martín-Vide, J., 2021. Perceptions of human thermal comfort in an urban tourism destination – a case study of Porto (Portugal). Build. Environ. 205, 108246. https://doi.org/10.1016/j.buildenv.2021.108246.
Lopes, H.S., Remoaldo, P.C., Ribeiro, V., Martín-Vide, J., 2022a. Pathways for adapting tourism to climate change in an urban destination – evidences based on thermal conditions for the Porto Metropolitan Area (Portugal). J. Environ. Manag. 315, 115161. https://doi.org/10.1016/j.jenvman.2022.115161.
Lopes, H.S., Remoaldo, P.C., Ribeiro, V., Martín-Vide, J., 2022b. A comprehensive methodology for assessing outdoor thermal comfort in touristic city of Porto (Portugal). Urban Clim. 45, 101264. https://doi.org/10.1016/j.uclim.2022.101264.
Lowry, W.P., 1977. Empirical estimation of urban effects on climate: a problem analysis. J. Appl. Meteorol. 16, 129–135. https://doi.org/10.1175/1520-0450(1977)016<0129:EEOUEO>2.0.CO;2.
McDonald, R.I., Aronson, M.F.J., Beatley, T., Beller, E., Bazo, M., Grossinger, R., Jessup, K., Mansur, A.V., Puppim de Oliveira, J.A., Panlasigui, S., Burg, J., Pevzner, N., Shanahan, D., Stoneburner, L., Rudd, A., Spotswood, E., 2023. Denser and greener cities: green interventions to achieve both urban density and nature. People and Nature 5 (1), 84–102. https://doi.org/10.1002/pan3.10423.
MacKerron, G., Mourato, S., 2009. Life satisfaction and air quality in London. Ecol. Econ. 68, 1441–1453. https://doi.org/10.1016/j.ecolecon.2008.10.004.
Martín, Y., Paneque, P., 2022. Moving from adaptation capacities to implementing adaptation to extreme heat events in urban areas of the European Union: introducing the U-ADAPT! research approach. J. Environ. Manag. 310, 114773. https://doi.org/10.1016/j.jenvman.2022.114773.
Meadowcroft, J., 2009. What about the politics? Sustainable development, transition management, and long term energy transitions. Policy Sci. 42, 323–340. https://doi.org/10.1007/s11077-009-9097-z.
Mears, M., Brindley, P., Maheswaran, R., Jorgensen, A., 2019. Understanding the socioeconomic equity of publicly accessible greenspace distribution: the example of Sheffield, UK. Geoforum 103, 126–137. https://doi.org/10.1016/j.geoforum.2019.04.016.
Monteiro, A., 1997. O clima urbano do Porto. Contribuição para a definição das estratégias de planeamento e ordenamento do território. Tese de Doutoramento em Geografia. Fundação Calouste Gulbenkian e Junta Nacional de Investigação Científica e Tecnológica, Lisboa.
Monteiro, A., Madureira, H., Fonseca, L., Velho, S., 2018. Revisão do Plano Diretor Municipal do Porto - Suporte Biofísico e Ambiente. Clima e Ambiente Urbano (Relatório de Caracterização e Diagnóstico). Porto.
Morabito, M., Crisci, A., Gioli, B., Gualtieri, G., Toscano, P., Di Stefano, V., Orlandini, S., Gensini, G.F., 2015. Urban-hazard risk analysis: mapping of heat-related risks in the elderly in major Italian cities. PLoS One 10. https://doi.org/10.1371/journal.pone.0127277.
Naboni, E., Natanian, J., Brizzi, G., Florio, P., Chokhachian, A., Galanos, T., Rastogi, P., 2019. A digital workflow to quantify regenerative urban design in the context of a changing climate. Renew. Sustain. Energy Rev. 113, 109255. https://doi.org/10.1016/j.rser.2019.109255.
Narimani, N., Karimi, A., Brown, R.D., 2022. Effects of street orientation and tree species thermal comfort within urban canyons in a hot, dry climate. Ecol. Inform. 69, 101671. https://doi.org/10.1016/j.ecoinf.2022.101671.
Norton, B.A., Coutts, A.M., Livesley, S.J., Harris, R.J., Hunter, A.M., Williams, N.S., 2015. Planning for cooler cities: a framework to prioritise green infrastructure to mitigate high temperatures in urban landscapes. Landsc. Urban Plann. 134, 127–138. https://doi.org/10.1016/j.landurbplan.2014.10.018.
Oke, T.R., 1982. The energetic basis of the urban heat island. Q. J. R. Meteorol. Soc. 108, 1–24. https://doi.org/10.1002/qj.49710845502.
Oke, T.R., 1987. The surface energy budgets of urban areas. In: American Meteorological Society. American Meteorological Society, New York, pp. 1–52. Modeling the Urban Boundary Layer.
Oke, T.R., Mills, G., Christen, A., Voogt, J.A., 2017. Urban Climates. Cambridge University Press, Cambridge.
Oliveira, A., Lopes, A., Correia, E., Niza, S., Soares, A., 2021. Heatwaves and summer urban heat islands: a daily cycle approach to unveil the urban thermal signal changes in Lisbon. Portugal. Atmosphere 12 (3), 292. https://doi.org/10.3390/atmos12030292.
Oliveira, G.M., Vidal, D.G., Ferraz, M.P., 2020. Urban lifestyles and consumption patterns. In: Filho, W.L., Azul, A.M., Brandli, L., Özuyar, P.G., Wall, T. (Eds.), Sustainable Cities and Communities. Encyclopedia of the UN Sustainable Development Goals. Springer, Nature Switzerland AG, Cham, pp. 851–860. https://doi.org/10.1007/978-3-319-71061-7_54-1.
Oliveira, S., Andrade, H., Vaz, T., 2011. The cooling effect of green spaces as a contribution to the mitigation of urban heat: a case study in Lisbon. Build. Environ. 46, 2186–2194. https://doi.org/10.1016/j.buildenv.2011.04.034.
Parastatidis, D., Mitraka, Z., Chrysoulakis, N., Abrams, M., 2017. Online global land surface temperature estimation from landsat. Remote Sens. 9. https://doi.org/10.3390/rs9121208.
Pauleit, S., Breuste, J.H., 2011. Land use and surface cover as urban ecological indicators. In: Niemelä, J., Breuste, J., Elmqvist, T., Guntenspergen, G., James, P., McIntyre, N. (Eds.), Urban Ecology: Patterns, Processes, and Applications. Oxford University Press, Oxford, pp. 19–30. https://doi.org/10.1093/acprof:oso/9780199563562.003.0004.
Porto Council, 2024. Municipality of Porto reinforces commitment to achieving carbon neutrality by 2030. https://www.porto.pt/pt/noticia/municipio-do-porto-reforca-compromisso-em-alcancar-a-neutralidade-carbonica-ate-2030. (Accessed 12 June 2024).
Santamouris, M., 2015. Analyzing the heat island magnitude and characteristics in one hundred Asian and Australian cities and regions. Sci. Total Environ. 512–513, 582–598. https://doi.org/10.1016/j.scitotenv.2015.01.060.
Semenzato, P., Bortolini, L., 2023. Urban heat island mitigation and urban green spaces: testing a model in the city of padova (Italy). Land 12. https://doi.org/10.3390/land12020476.
Senanayake, I.P., Welivitiya, W.D.D.P., Nadeeka, P.M., 2013. Urban green spaces analysis for development planning in Colombo, Sri Lanka, utilising THEOS satellite imagery - a remote sensing and GIS approach. Urban For. Urban Green. 12, 307–314. https://doi.org/10.1016/j.ufug.2013.03.011.
Shafizadeh-Moghadam, H., Weng, Q., Liu, H., Valavi, R., 2020. Modeling the spatial variation of urban land surface temperature in relation to environmental and anthropogenic factors: a case study of Tehran, Iran. GIScience Remote Sens. 57, 483–496. https://doi.org/10.1080/15481603.2020.1736857.
Shih, W.Y., 2022. Socio-ecological inequality in heat: the role of green infrastructure in a subtropical city context. Landsc. Urban Plann. 226. https://doi.org/10.1016/j.landurbplan.2022.104506.
Silva, L.T., Mendes, J.F.G., 2012. City Noise-Air: an environmental quality index for cities. Sustain. Cities Soc. 4, 1–11. https://doi.org/10.1016/j.scs.2012.03.001.
Silva, L.T., 2015. Environmental quality health index for cities, Hab. Intern 45 (P1), 29–35. https://doi.org/10.1016/j.habitatint.2014.06.020.
Song, Z., Li, R., Qiu, R., Liu, S., Tan, C., Li, Q., Ge, W., Han, X., Tang, X., Shi, W., Song, L., Yu, W., Yang, H., Ma, M., 2018. Global land surface temperature influenced by vegetation cover and PM2.5 from 2001 to 2016. Remote Sens. 10, 2034. https://doi.org/10.3390/rs10122034.
Taha, H., 1997. Urban climates and heat islands: albedo, evapotranspiration, and anthropogenic heat. Energy Build. 25, 99–103. https://doi.org/10.1016/s0378-7788(96)00999-1.
Tam, B.Y., Gough, W.A., Mohsin, T., 2015. The impact of urbanisation and the urban heat island effect on day to day temperature variation. Urban Clim. 12, 1–10. https://doi.org/10.1016/j.uclim.2014.12.004.
Tara, K., Singh, S., Kumar, R., 2015. Green banking for environmental management: a paradigm shift. Curr. World Environ. 10, 1029–1038. https://doi.org/10.12944/cwe.10.3.36.
Tomlinson, C.J., Chapman, L., Thornes, J.E., Baker, C.J., 2011. Including the urban heat island in spatial heat health risk assessment strategies: a case study for Birmingham, UK. Int. J. Health Geogr. 10, 42. https://doi.org/10.1186/1476-072X-10-42.
Tzoulas, K., Korpela, K., Venn, S., Yli-Pelkonen, V., Kaźmierczak, A., Niemela, J., James, P., 2007. Promoting ecosystem and human health in urban areas using Green Infrastructure: a literature review. Landsc. Urban Plann. https://doi.org/10.1016/j.landurbplan.2007.02.001.
Upmanis, H., Eliasson, I., Lindqvist, S., 1998. The influence of green areas on nocturnal temperatures in a high latitude city (Goteborg, Sweden). Int. J. Climatol. 18, 681–700. https://doi.org/10.1002/(SICI)1097-0088(199805)18:6<681::AID-JOC289>3.0.CO;2-L.
van Oorschot, J., Slootweg, M., Remme, R.P., et al., 2024. Optimizing green and gray infrastructure planning for sustainable urban development. npj Urban Sustain 4, 41. https://doi.org/10.1038/s42949-024-00178-5.
Vidal, D.G., Dias, R.C., Teixeira, C.P., Fernandes, C.O., Filho, W.L., Barros, N., Maia, R.L., 2022a. Clustering public urban green spaces through ecosystem services potential: a typology proposal for place-based interventions. Environ. Sci. Pol. 132, 262–272. https://doi.org/10.1016/j.envsci.2022.03.002.
Vidal, D.G., Fernandes, C.O., Viterbo, L.M.F., Vilaça, H., Barros, N., Maia, R.L., 2021. Combining an evaluation grid application to assess ecosystem services of urban green spaces and a socioeconomic spatial analysis. Int. J. Sustain. Dev. World Ecol. 28, 291–302. https://doi.org/10.1080/13504509.2020.1808108.
Vidal, D.G., Maia, R.L., Oliveira, G.M., Pontes, M., Barreira, E., 2019. Cities challenges in the contemporary societies: urban sustainability and environmental issues. Sociol. LINE, Rev. da Assoc. Port. Sociol. 20, 119–138. https://doi.org/10.30553/sociologiaonline.2019.20.
Vidal, D.G., Oliveira, G.M., Pontes, M., Maia, R.L., Ferraz, M.P., 2022b. The influence of social and economic environment on health. In: Prata, J.C., Isabel, A. (Eds.), One Health. Elsevier, Amsterdam, pp. 205–229. https://doi.org/10.1016/b978-0-12-822794-7.00005-8.

Weng, Q., 2009. Thermal infrared remote sensing for urban climate and environmental studies: methods, applications, and trends. ISPRS J. Photogramm. Remote Sens. 64, 335–344. https://doi.org/10.1016/j.isprsjprs.2009.03.007.

Wisner, B., 2016. Vulnerability as concept, model, metric, and tool. In: Oxford Research Encyclopedia of Natural Hazard Science. Oxford Research Encyclopedias, Oxford, pp. 1–51. https://doi.org/10.1093/acrefore/9780199389407.013.25.

World Health Organization, 2010. In: Europe, W.R. O.f. (Ed.), Urban Planning, Environment and Health: from Evidence to Policy Action, p. 119.

Wu, Z., Zhang, Y., 2019. Water bodies' cooling effects on urban land daytime surface temperature: ecosystem service reducing heat island effect. Sustain. Times 11. https://doi.org/10.3390/su11030787.

Yang, X., Zhao, C., Zhou, L., Wang, Y., Liu, X., 2016. Distinct impact of different types of aerosols on surface solar radiation in China: variation of Aerosol Radiative Effect. J. Geophys. Res. Atmospheres 121, 6459–6471. https://doi.org/10.1002/2016JD024938.

Zhu, D., Zhou, X., Cheng, W., 2022. Water effects on urban heat islands in summer using WRF-UCM with gridded urban canopy parameters — a case study of Wuhan. Build. Environ. 225. https://doi.org/10.1016/j.buildenv.2022.109528.

Ziter, C.D., Pedersen, E.J., Kucharik, C.J., Turner, M.G., 2019. Scale-dependent interactions between tree canopy cover and impervious surfaces reduce daytime urban heat during summer. Proc. Natl. Acad. Sci. U.S.A. 116 (15), 7575–7580. https://doi.org/10.1073/pnas.1817561116.